

Accepted Manuscript

Phosphorus cycling in Lake Cadagno, Switzerland: A low sulfate euxinic ocean analogue

Yijun Xiong, Romain Guilbaud, Caroline L. Peacock, Raymond P. Cox, Donald E. Canfield, Michael D. Krom, Simon W. Poulton

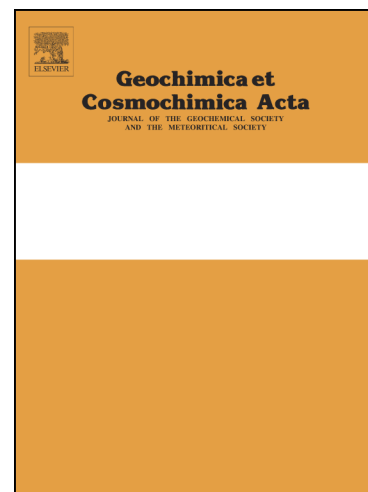
PII: S0016-7037(19)30088-2
DOI: <https://doi.org/10.1016/j.gca.2019.02.011>
Reference: GCA 11126

To appear in: *Geochimica et Cosmochimica Acta*

Received Date: 29 November 2017
Revised Date: 5 February 2019
Accepted Date: 6 February 2019

Please cite this article as: Xiong, Y., Guilbaud, R., Peacock, C.L., Cox, R.P., Canfield, D.E., Krom, M.D., Poulton, S.W., Phosphorus cycling in Lake Cadagno, Switzerland: A low sulfate euxinic ocean analogue, *Geochimica et Cosmochimica Acta* (2019), doi: <https://doi.org/10.1016/j.gca.2019.02.011>

This is a PDF file of an unedited manuscript that has been accepted for publication. As a service to our customers we are providing this early version of the manuscript. The manuscript will undergo copyediting, typesetting, and review of the resulting proof before it is published in its final form. Please note that during the production process errors may be discovered which could affect the content, and all legal disclaimers that apply to the journal pertain.



Phosphorus cycling in Lake Cadagno, Switzerland: A low sulfate euxinic ocean analogue

Yijun Xiong^{1*}, Romain Guilbaud², Caroline L. Peacock¹, Raymond P. Cox³,
Donald E. Canfield³, Michael D. Krom^{1,4}, Simon W. Poulton^{1*}

¹School of Earth and Environment, University of Leeds, Leeds LS2 9JT, UK

²Lancaster Environment Centre, Lancaster University, Lancaster, LA1 4YQ, UK

³Institute of Biology, University of Southern Denmark, Campusvej 55, 5230 Odense M,
Denmark

⁴Charney School of Marine Sciences, Haifa University, Rehov Aba Koushy, Haifa, Israel

*Corresponding authors: eeyx@leeds.ac.uk; s.poulton@leeds.ac.uk

Abstract

Low sulfate, euxinic water-column conditions were a common feature of many Precambrian and Phanerozoic periods of ocean anoxia. The cycling of phosphorus in anoxic marine environments exerts a fundamental control on primary productivity, organic carbon production and burial, and hence ultimately oxygen production, but the dynamics of the phosphorus cycle in low sulfate, euxinic settings are largely unknown. Here, we provide a detailed geochemical investigation of phosphorus cycling in the low sulfate, euxinic Lake Cadagno, Switzerland, which is considered a prime analogue for ancient euxinic oceans. We find evidence for extensive recycling of phosphorus from the sediments back to the water column, stimulated by the microbial release of phosphorus from organic matter and Fe (oxyhydr)oxide minerals. Consistent with previous studies of modern and ancient anoxic settings, this regenerated flux maintains high concentrations of phosphorus in the water column, thus promoting a positive productivity feedback. However, the low-sulfate condition of the overlying water column, combined with the rapid removal of sulfide (as pyrite) from porewaters, promotes formation of Fe(II) phosphate minerals (e.g., vivianite) close to the sediment-water interface. This, in turn, modulates the extent of phosphorus recycling back to the water column, and contrasts with modern fully marine euxinic settings, where the higher concentrations of dissolved sulfate promote sulfide formation to greater depths, thus limiting Fe(II) phosphate formation close to the sediment-water interface. The prevalence of low-sulfate conditions during past euxinic episodes suggests that the operation of this near-surface sedimentary trap for recycled phosphorus would have limited the positive P-driven productivity feedback, promoting only a moderate degree of P recycling. Furthermore, the precise magnitude of this recycled P flux would, on a global scale, have been dependent on changes in the size of Earth's marine sulfate reservoir through time. Thus our findings have major implications for rates of P-driven productivity and organic carbon burial in ancient euxinic settings, which have not previously been factored into reconstructions of Earth's oxygenation history.

1. INTRODUCTION

Euxinic (sulfidic) water column conditions were an important feature during periods of ocean anoxia throughout much of Earth's history. Evidence for spatially and temporally restricted episodes of ocean euxinia date back to at least ~2.7 billion years ago (Ga), with such conditions early in Earth's history often being linked to an increased oceanic influx of sulfate due to oxidative weathering of pyrite as atmospheric oxygen rose (Reinhard et al.,

2009; Kendall, et al., 2010; Scott et al., 2011). Euxinic conditions are generally considered to have become more widespread in the mid-Proterozoic, from ~1.84 to 1.0 Ga, with euxinia being particularly prevalent along productive continental margins and in epicontinental seas (Canfield, 1998; Poulton et al., 2004a; 2010; Scott et al., 2008; Poulton and Canfield, 2011). Euxinic episodes through the Neoproterozoic were more scarce, and instead anoxic ferruginous (Fe containing) water column conditions tended to dominate (Canfield et al., 2008; Johnston et al., 2010; Guilbaud et al., 2015; Sperling et al., 2015), although euxinic conditions did occur at certain times in some Neoproterozoic basins (e.g., Canfield et al., 2008; Li et al., 2010; 2012; Sahoo et al., 2012; Guilbaud et al., 2015; Thomson, et al., 2015; Och et al., 2016). Widespread euxinia has also been reported for certain intervals of the Paleozoic (e.g., Wignall and Twitchett, 1996; Wignall et al., 2010; Gill et al., 2011; Hammarlund et al., 2012), and during the oceanic anoxic events (OAEs) of the Mesozoic (e.g., Jenkyns, 2010).

A common feature of Precambrian euxinic episodes concerns the prevalence of relatively low marine sulfate concentrations compared to the modern ocean (~28 mM), which from the early Proterozoic to the terminal Neoproterozoic likely increased from the low micromolar range envisaged for much of the earlier Archean (Habicht et al., 2002; Crowe et al., 2014), to concentrations in the low millimolar range (Kah et al., 2004; Guilbaud et al., 2015). Similarly, a growing body of evidence suggests that sulfate concentrations were also much lower than at present during many Phanerozoic periods of euxinia (in the low millimolar range), at least through to (and including) the anoxic episodes of the Jurassic and Cretaceous (e.g., Adams et al., 2010; Newton et al., 2011; Song et al., 2013; Poulton et al., 2015).

Despite the significance of low-sulfate euxinic settings through time, relatively little is known about controls on P cycling under such conditions. P is commonly invoked as the ultimate limiting nutrient on geologic timescales, with the behaviour of bioavailable P exerting a major control on primary productivity and hence organic carbon burial (e.g., Howarth, 1988; Tyrell, 1999). These factors ultimately exert a primary control on Earth's oxygenation history (e.g., Canfield, 2005), and it has been suggested that prior to Earth's first major rise in atmospheric oxygen (the Great Oxidation Event from ~2.45-2.32 Ga), bioavailable P was limited in the ocean due to removal via extensive adsorption to Fe (oxyhydr)oxides under anoxic ferruginous water column conditions (Bjerrum and Canfield, 2002; Jones et al., 2015; Reinhard et al., 2017; but see Konhauser et al., 2007; Planavsky et al., 2010).

After the Great Oxidation Event (GOE) at ~2.4-2.2 Ga, atmospheric oxygen levels are believed to have remained relatively stable (but with concentrations much lower than at present) under the more widespread euxinic conditions envisaged from ~1.84-1.0 Ga (Canfield, 2005; Lyons et al., 2014; Planavsky et al., 2014; Zhang et al., 2016; Daines et al., 2017). However, nutrient controls on productivity (and hence oxygen stability) across this mid-Proterozoic interval remain unclear. Limitation of the N cycle due to extensive Mo drawdown to the sediment coupled with enhanced loss of fixed N as N₂ (Anbar and Knoll, 2002; Fennel et al., 2005; Canfield et al., 2006; Scott et al., 2008; but also see Zerkle et al., 2006), or an increased contribution of anoxygenic photosynthesis to total primary production (Johnston et al., 2009), have been proposed as mechanisms to limit O₂ production in the mid-Proterozoic euxinic ocean. However, recent isotopic studies of the mid-Proterozoic N cycle suggest that bioavailable nitrate was likely abundant in near-shore environments (Godfrey et al., 2013; Stüeken, 2013; Koehler et al., 2017), while research on modern ferruginous systems implies that large expanses of the mid-Proterozoic ocean were likely P, and not N, limited (Michiels et al., 2017). In this regard, based on the total P content of shallow water marine shales through time, Reinhard et al. (2017) suggest that bioavailable P was maintained at extremely low concentrations throughout the mid-Proterozoic due to extensive stripping of water column P in association with Fe (oxyhydr)oxide minerals formed under deeper-water ferruginous conditions. Extremely low bioavailable P would have ultimately maintained atmospheric oxygen at low levels throughout the mid-Proterozoic (Reinhard et al., 2017). However, this assertion assumes that the total P content of shallow marine shales provides a direct record of bioavailable P in the water column, with insignificant biogeochemical recycling of P from sediments back to the water column (Poulton, 2017).

The extent to which bioavailable P may be trapped in the sediment, as opposed to being recycled back to the water column (where it can fuel further productivity), is highly redox dependent. In organic-rich sediments deposited beneath oxic bottom waters, P is typically delivered to the sediment in association with organic matter and/or iron (oxyhydr)oxide minerals, in addition to detrital phases. During early diagenesis, organic matter and Fe (oxyhydr)oxide remineralisation (partially) releases P to pore waters (Krom and Berner, 1981; Froelich et al., 1988; Slomp et al., 1996b; Anschutz et al., 1998), with the potential either for recycling of some of this P to the overlying water column (Ingall and Jahnke, 1994; 1997; Slomp et al., 2002; 2004), or for the fixation of P in the sediment in association with other phases (i.e., sink-switching) (Van Cappellen and Ingall, 1994; Slomp et al., 1996a, b). Using a sequential P extraction technique, Ruttenberg and Berner (1993) demonstrated that a large

proportion of the released P may be fixed as authigenic carbonate fluorapatite (CFA), and this is believed to typically account for ~50% of P burial in modern marine sediments deposited beneath oxic bottom waters. In addition, some of the recycled porewater P may be trapped in the sediment via re-adsorption to Fe (oxyhydr)oxide minerals close to the sediment-water interface (Slomp and Van Raaphorst, 1993; Slomp et al., 1996a, b; Dellwig et al., 2010).

Although these processes may begin in the oxic water column via the oxic degradation of organic matter, water column P recycling and the release of P from sediment porewaters tends to be particularly significant under euxinic conditions. In particular, the Fe (oxyhydr)oxide sink for P is greatly diminished under such conditions due to the reductive dissolution of Fe (oxyhydr)oxide minerals by dissolved sulfide (e.g., Pyzik and Sommer, 1981; Dos Santos Afonso and Stumm, 1992; Peiffer et al., 1992; Poulton, 2003; Poulton et al., 2004b) and the ultimate formation of pyrite, to which phosphate does not significantly adsorb (Krom and Berner, 1980; Anschutz et al., 1998). The effect of diminishing this sink under euxinic conditions is exacerbated by the preferential release of P from organic matter during microbial remineralisation (e.g., during the production of sulfide via bacterial sulfate reduction), which ultimately results in high organic C/P ratios relative to the Redfield Ratio (e.g., Ingall et al., 1993; Steenbergh et al., 2011).

The formation of ferrous phosphate minerals (e.g., vivianite) has been proposed as an additional potential sink for reactive phosphate during early diagenesis. For example, Fe(II) phosphate has been implicated as a significant retention mechanism for P in Lake Ørn, Denmark (O'Connell et al., 2015) and Lake GroßGlienicke, Germany (Rothe et al., 2014). Both lakes are oxic, but the deeper sediment pore waters are characterised by high concentrations of dissolved Fe^{2+} , and in these deep sediments the phosphate released from organic matter remineralization and Fe (oxyhydr)oxide reduction can re-precipitate as vivianite. Similarly, Fe(II) phosphate has been suggested as a prominent sink for P in a variety of coastal and deep-sea oxic water-column settings. Here, in sulfide-depleted sediments beneath the sulfate/methane transition zone (SMT; where porewater sulfate is depleted and methane concentrations increase), Fe (oxyhydr)oxide mineral reduction either via dissimilatory Fe reduction or via anaerobic oxidation of methane (AOM) using Fe (oxyhydr)oxides as the electron acceptor (Konhauser et al., 2005; Thauer and Shima, 2008; Riedinger et al., 2014), and the availability of dissolved phosphate appears to promote vivianite formation (e.g., März et al., 2008a; Slomp et al., 2013; Hsu et al., 2014; Egger et al., 2015).

In addition, vivianite formation has been proposed to occur in a variety of anoxic water-column settings, including sediments of the Baltic Sea, in both the deeper euxinic basins (Jilbert and Slomp, 2013) and potentially in the intermittently anoxic Landsort Deep basin (Dijkstra et al., 2016), as well as in the seasonally anoxic Chesapeake Bay (Berner, 1990; Joshi et al., 2015) and in the euxinic Black Sea (Dijkstra et al., 2014). In all of these cases, vivianite has been suggested to form in microenvironments within shallow sulfidic sediments. However, Kraal et al. (2017) demonstrated that vivianite is rapidly dissolved via reaction with sulfide, and at least in the case of the euxinic Black Sea, the remobilised phosphate is more likely associated with carbonate minerals, rather than precipitated as vivianite (see also Dijkstra et al., 2018). Thus the significance of vivianite formation as a longer-term trap for remobilised P in these modern sulfidic porewater environments is unclear.

Although active formation of vivianite has been demonstrated in a variety of settings, these environments are not particularly relevant analogues for the low-sulfate euxinic oceans of the Precambrian and Phanerozoic. In particular, while the limited availability of sulfate (and hence sulfide) during diagenesis in ancient low-sulfate euxinic settings could conceivably promote formation of vivianite, the importance of Fe(II) phosphate formation relative to the extent of P recycling back to the water column remains unknown. In addition to the potential significance for the history of planetary oxygenation during the Precambrian, a detailed understanding of biogeochemical controls on P recycling under low-sulfate euxinic conditions is of key importance for evaluating productivity feedbacks during Phanerozoic episodes of euxinia (e.g., Mort et al., 2007; März et al., 2008b; Poulton et al., 2015).

Lake Cadagno, Switzerland, has been the focus of considerable research, largely due to its significance as a mid-Proterozoic euxinic ocean analogue (Canfield et al., 2010; Dahl et al., 2010; Wirth et al., 2013). The lake represents an ideal location to study P cycling in relation to ancient euxinic settings as it is persistently euxinic at depth, with a relatively low sulfate content of 1.2 mM. In addition, the remote location of Lake Cadagno ensures insignificant anthropogenic phosphorus pollution, and phosphate concentrations in the water column (0.1-2 μM) tend to be lower than in other euxinic or seasonally euxinic settings, such as the Black Sea (2-7 μM) (Codispoti et al., 1991; Yakushev et al., 2008; Dellwig et al., 2010) and the Baltic Sea (3-5 μM) (Dellwig et al., 2010).

Here, we provide new water column and sediment data for Lake Cadagno, focusing on different parts of the basin, including the deeper euxinic waters, shallower oxic waters, and a site where the chemocline intersects the deposited sediments. We combine Fe and P speciation data with bulk geochemical analyses, to assess controls on P recycling under low-

sulfate euxinic conditions. We specifically highlight the role of P recycling back to the water column, with a focus on the potential modulation of this flux by the early diagenetic formation of Fe(II) phosphate minerals.

2. SAMPLING AND METHODS

2.1. Sample location and geological setting

Lake Cadagno is a meromictic lake located at approximately 2000 m altitude in the central Alps of Switzerland (46°33'44''N, 8°42'41''E; Fig. 1). The bedrock includes felsic gneiss, dolomite and gypsum (Dahl et al., 2010). The basin is 0.26 km² with a maximum depth of 21 m (Krige, 1917). The water column is stratified, with oxic surface waters above the chemocline overlying euxinic deeper waters. This stratification has developed due to different densities of water flowing into the lake (Tonolla et al., 1998). Specifically, the oxic mixolimnion occurs at depths from 0 to 11 m and is fed by surface runoff. The euxinic bottom waters occur from 12 to 21 m depth, and these waters are supplied by deep sub-surface flow containing a high concentration of ions, including dissolved sulfate concentrations in the range of 5 to 8 mM (Del Don et al., 1998; 2001). The oxic surface waters and deep sulfidic waters are separated by a chemocline of about 1 meter thickness (Tonolla et al., 1998; 1999). Sedimentation in the lake has occasionally been affected by landslides (Knoll-Heitz, 1991; Birch et al., 1996), which we consider in more detail below.

2.2. Water column, pore water and sediment sampling

Samples were collected in summer 2014 over the course of two days. All water column samples, as well as sediment samples from beneath the euxinic deeper waters, were taken from a permanently moored platform, while sediment samples beneath oxic waters and from where the chemocline intersects the sediment towards the edge of the lake were taken from a boat. Water column samples from the oxic, chemocline and deeper euxinic waters were collected by pumping from depth into expandable plastic containers, which were previously purged with N₂. Immediately after collection, water samples were filtered in a N₂ filled glove bag for immediate analysis of dissolved Fe(II) and phosphate, while dissolved sulfide was determined after fixing sulfide with 10 mM zinc acetate.

Short (up to 35 cm) gravity cores were taken from 3 different water depths: one representing deposition under euxinic conditions (20-21 m; euxinic core), another where the chemocline intersects the lake bottom (11-12 m; chemocline core), and a third in oxic waters

(5-6 m; oxic core) (Fig. 1). After sampling, cores were stored upright and refrigerated at 4°C prior to processing (which occurred within 6 h). Sediment cores were sliced (generally in thicknesses of 1-2 cm) in the glove bag and placed in 50 mL centrifuge tubes. Pore water was extracted from each sample while still in the glove bag using rhizon ceramic filters (Rhizosphere research products). Pore waters were then fixed in the appropriate reagent for Fe²⁺ and phosphate analysis (see below) while still in the glove bag, and were then analysed immediately after opening the glove bag. Sulfide samples were fixed in 10 mM Zn acetate while still in the glove bag and analysed later. Sediment samples were immediately frozen after opening the glove bag, and were subsequently freeze-dried and stored frozen in an anoxic chamber prior to analysis.

2.3. Water content

To determine the water content of the sediments, frozen cores sampled adjacent to the cores used for geochemical analysis were sliced with an electric saw (generally in thicknesses of 1-2 cm) and each slice was dried at 100°C overnight. The weight loss was then used to calculate water content (Birch et al., 1996). This was only performed for the euxinic and chemocline cores, to investigate the extent to which these sediments have been affected by landslides (see below).

2.4. Geochemical methods

2.4.1 Water column and pore water analysis

Immediately after filtration of both lake waters and pore waters, pH was measured with a calibrated pH meter (Mettler Toledo AG 8603). Dissolved Fe(II) concentrations were measured via the ferrozine method with a RSD of <2% (Stookey, 1970; Viollier et al., 2000). Dissolved P was measured via the molybdate blue method with a RSD of <3% (Koroleff, 1976; Ruttenberg, 1992). Dissolved sulfide was measured using the Cline method, with a RSD of <2% (Cline, 1969). For the measurement of dissolved sulfate, 2.5 mL of sample was treated with 100 µl of 10 mM zinc acetate to remove the sulfide by filtration, then the filtrates were analysed by ion chromatography using a Dionex IonpacTM AS16 column with a RSD of <2%. Dissolved inorganic carbon (DIC) was measured using flow injection analysis (Hall, 1992) with a RSD of <1%.

2.4.2 Sediment analysis

Total carbon (TC), total organic carbon (TOC) and total sulphur (TS) were measured with a LECO C/S Analyzer. TOC samples were pre-treated with 10% HCl to remove carbonate phases. Replicate analyses of certified standards (Soil 502-309, Soil 502-062, Calcium carbonate 501-034 and Coal 502-671) gave RSDs of <2% for TC, <2% for TOC, and <4% for TS, with 100% recovery in all cases. Total inorganic carbon (TIC) was calculated as $TIC = TC - TOC$, and replicates of TIC analyses gave a RSD of <2%. Total Fe, Al, Ti and P were determined following total digestion of the freeze-dried sediment samples, whereby samples were initially ashed at 550°C, and then dissolved in HNO_3 -HF- $HClO_4$ followed by evaporation to dryness. Boric acid was then added and evaporated to dryness overnight (to solubilise aluminium hexafluoride), and finally the sample was re-dissolved in hot HNO_3 . Total Fe (Fe_T) was measured by AAS, while Al and Ti were measured by ICP-OES, and Total P (P_T) was measured by spectrophotometer using the molybdate blue method, as described above. Replicate analyses of a Lake Cadagno sediment sample gave RSDs of <2% for all four elements, and replicate analyses of international sediment standard PACS-2 gave recoveries of 98%, 96%, 93% and 100% for Fe, Al, Ti and P, respectively.

The Fe extraction methods were developed from Poulton and Canfield (2005) and Canfield et al. (1986), as used by Zegeye et al. (2012) and Goldberg et al. (2012). Together, the procedure targets six operationally-defined phases, with steps I-III performed sequentially (for extraction details see Table 1, which also reports target Fe phases and the precision of each extraction based on replicate extractions). Iron extracted from unsulfidized reduced Fe phases ($Fe(II)_{unsulf}$) (Table 1) was measured by spectrophotometer via the ferrozine method (Stookey, 1970), while the other unsulfidized Fe phases were measured by AAS. Sulfide bound as acid-volatile sulfur (Fe_{AVS}) and pyrite (Fe_{py}) was extracted by the two-step acid Cr(II) method and trapped as Ag_2S , followed by weighing of the precipitate and stoichiometric conversion to Fe concentrations (Canfield et al., 1986; Fossing and Jorgensen, 1989).

The pool of easily reducible ferric oxides such as ferrihydrite ($Fe(III)_{ox1}$) was calculated as the difference between the total Fe extracted by the 0.5 N HCl extraction (i.e., Fe(II) plus Fe(III)) and the Fe(II) measured in this extract (Goldberg et al., 2012; Zegeye et al., 2012). Because Fe_{AVS} is also extracted by the 0.5 N HCl extraction and measured as Fe(II) (Poulton and Canfield, 2005), the unsulfidized solid phase Fe(II) was calculated from the Fe(II) extracted by 0.5 N HCl after subtracting Fe_{AVS} . The total pool of Fe that is considered highly reactive (Fe_{HR}) to biotic and abiotic reduction in the euxinic water column and during early

diagenesis (Canfield et al., 1992; Raiswell and Canfield, 1998; Poulton et al., 2004a) was calculated as:

$$Fe_{HR} = Fe(II)_{unsulf} + Fe(III)_{ox1} + Fe(III)_{ox2} + Fe_{mag} + Fe_{AVS} + Fe_{py} \quad (1)$$

The sequential extraction method (SEDEX) for different phosphorus phases was modified from Ruttenberg (1992). Five sedimentary P reservoirs were extracted by different reagents as detailed in Table 2. Iron-bound P (P_{Fe}) was determined via the molybdate blue method (Koroleff, 1976), after suitable dilution with matrix-matched standards, on a SEAL Analytical AA3 segmented flow analyser. All other P phases were determined via the molybdate blue method on a Thermo Genesys 6 spectrophotometer at 880 nm wavelength. Reactive P ($P_{reactive}$) was calculated as:

$$P_{reactive} = P_{sorb} + P_{Fe} + P_{auth} + P_{org} \quad (2)$$

Fe(II) phosphate (e.g., vivianite) was not part of the mineral suite tested during development of the SEDEX procedure (Ruttenberg, 1992). To address this we first synthesized vivianite by the method of Madsen and Hansen (2014), whereby 100 mL of 0.1 M NaH_2PO_4 was titrated into 250 mL of 0.025 M $(NH_4)_2Fe(SO_4)_2$, with the pH maintained at 7 using 0.5 M NaOH. The whole operation was completed under anoxic conditions and the product was subsequently characterised as vivianite by X-ray diffraction (XRD). Then we applied the first stages of the Fe and P sequential procedures and found that vivianite was completely dissolved by citrate/dithionite/bicarbonate (CDB) in the P extractions (Table 2, Step II; see also Dijkstra et al., 2014; Kraal et al., 2017), and by 0.5 M HCl in the Fe extractions (Table 1, Step I).

2.5 Geochemical modelling

The saturation indexes (SI) of porewater with respect to vivianite, siderite and pyrite were calculated using PHREEQC Interactive 3.3.7, utilising the databases of Laliberté (2009) and Appelo et al. (2014). The SI calculations were based on porewater data for the euxinic core, including pH and the concentrations of Fe^{2+} , HPO_4^{2-} , total sulfide, and DIC. Calculations were performed for a temperature of 4°C (Dahl et al., 2010) and redox potential (Eh) of -300 mV, which correspond to values measured at the sediment-water interface (Gregersen et al., 2009; Dahl et al., 2010). Eh-pH mineral stability fields were calculated for a temperature of 4°C using Geochemist's Workbench 11.0. The input data were based on the euxinic core porewater data for Fe^{2+} , SO_4^{2-} , HPO_4^{2-} and HCO_3^- at 0-5 cm and 29.5-31.5 cm.

The concentrations of HPO_4^{2-} and HCO_3^- were 25.74 μM and 3.75 mM in the surface sediments, and 24.83 μM and 5.11 mM in the deeper sediments, respectively, which were calculated from DIC and total dissolved P using PHREEQC.

3. RESULTS

3.1. Water column

All geochemical data are presented in Appendix A. The water column is supersaturated with oxygen to a depth of ~7 m, below which the oxygen starts to decrease rapidly, with near-complete removal at ~11 m (Fig. 2a). Dissolved sulfate concentrations increase with depth due to the input from subterranean springs (Fig. 1), with concentrations reaching 1.2 mM below the chemocline (Fig. 2b). Dissolved Fe^{2+} is low in concentration from the surface water to the chemocline (Fig. 2c). However, from 11 to 12 m, its concentration increases slightly to 1.1 μM just below the chemocline, with relatively constant concentrations below this depth. Dissolved sulfide increases in concentration below the chemocline, but remains relatively constant at $65 \pm 5 \mu\text{M}$ below ~13 m depth. Dissolved phosphate is low in surface waters, but progressively increases to ~2 μM with depth below the chemocline (Fig. 2d).

3.2. Sediment water content

The water content of Lake Cadagno sediments was used to constrain the depth interval where normal sedimentation has been affected by landslides (Birch et al., 1996). In the euxinic sediment core (Fig. 3a), the water content decreases with depth, but with a pronounced deviation to lower values between 12-18.5 cm. This corresponds to the position of a previously identified landslide layer (Birch et al., 1996) that was deposited in 1951 (Knoll-Heitz, 1991). Birch et al. (1996) also found evidence for an older landslide of ~12 cm thickness starting about 4 cm below the first landslide interval. We see no evidence for this earlier landslide based on the water content of the euxinic core between 18.5-23 cm, but based on a number of geochemical indicators (see below) we place the upper boundary of this earlier landslide interval at ~22.5 cm.

The chemocline core (Fig. 3b) shows a similar overall decrease in water content with depth, with a clear deviation to lower water content between 12-26 cm, although a return to slightly higher water content occurs at about 14-16.5 cm. This trend suggests that the interval from 12-26 cm captures the landslides outlined above. The oxic core was sampled from shallower water at the opposite side of the lake from where the landslides originated. The

lack of any discrepancies in geochemical data trends (see below) confirms that this core is unlikely to have been affected by any of the landslides.

3.3. Pore waters

DIC and pH were measured in the porewaters of the euxinic core in order to calculate mineral saturation indices. DIC shows an overall increase to a depth of ~15 cm, then remains constant at 5.42 ± 0.15 mM (Fig. 4). The pH shows a similar depth profile to DIC with an increase to ~14 cm, below which values are relatively constant at 8.42 ± 0.04 (Fig. 4).

In the euxinic sediment core (Fig. 5a), sulfate is relatively constant at 485 ± 5 μ M to a depth of 9 cm, which is likely due to some mixing of poorly-consolidated organic-rich ooze which comprised the top few cm of the core. Below 9 cm depth, sulfate is depleted to close to zero at a depth of 26 cm. Dissolved sulfide (Fig. 5a) is significantly higher than in the overlying water column (Fig. 2c) and shows an overall increase, reaching ~900 μ M at ~11 cm depth. Sulfide then decreases to close to zero at 26 cm as sulfate is depleted. At this depth dissolved Fe^{2+} begins to accumulate, reaching 35 μ M at 30 cm depth. Dissolved phosphate shows an overall increase to ~55 μ M over the top 12 cm, followed by a gradual decrease through the lower part of the core, although concentrations remain above 40 μ M at 30 cm depth.

In the chemocline core, sulfate concentrations decrease from >1 mM near the surface to much lower values below 20 cm, although concentrations do not reach zero (Fig. 5c). Sulfide steadily decreases with sediment depth from ~500 μ M close to the sediment-water interface, but in contrast to the euxinic core, sulfide only decreases to ~70 μ M at 23 cm depth. As a consequence, dissolved Fe^{2+} is present at low levels throughout the core (Fig. 5d). Dissolved phosphate shows a similar profile to the euxinic core, with a slight rise to ~21 μ M at 8 cm, followed by a gradual decrease with depth.

In the oxic core, sulfate is relatively low throughout (<200 μ M) and decreases with depth, although as with the chemocline core, values do not reach zero (Fig. 5e). Dissolved sulfide remains relatively constant at 230 ± 40 μ M, and this buffers dissolved Fe^{2+} , which remains close to zero throughout the core (Fig. 5f). As with the euxinic and chemocline cores, dissolved phosphate initially increases slightly, to ~42 μ M at 7.5 cm depth. However, after a slight decrease, dissolved phosphate then remains relatively constant at 38 ± 2 μ M.

3.4. Sediment geochemistry

3.4.1 Bulk composition

The concentration of TIC generally decreases with depth in each core (Fig. 6), to values close to zero at ~19 cm in the euxinic core and ~16 cm in the chemocline core, although TIC remains somewhat higher throughout the oxic core. TOC concentration is high in the upper samples of all cores (Fig. 6), reaching more than 10 wt% in the euxinic and chemocline cores, and almost 20 wt% close to the sediment-water interface in the oxic core. The oxic core shows a steady down-core decrease in TOC due to microbial remineralization, whereas the more sudden decreases evident at depth in the euxinic and chemocline cores (Fig. 6) likely reflect additional dilution by landslide sediment. However, TOC concentrations at depth in the euxinic and chemocline cores generally remain above ~2 wt%.

Total sulfur concentration fluctuates significantly in the euxinic core, with transitions to lower values evident in the depth sections affected by landslides (Fig. 6). By contrast, TS shows a more stable profile in the chemocline and oxic cores, with an overall slight decrease with depth from ~2.5 wt% close to the sediment-water interface. Total Fe increases from ~3.6 wt% at the surface, to a peak of ~8.0 wt% at 21 cm in the euxinic core, followed by a subsequent decrease (Fig. 6). In the chemocline and oxic cores, total Fe concentrations are lower and increase slightly with depth, but below ~20 cm in the chemocline core there is a slight decrease, similar to the euxinic core.

The detrital elements Al and Ti show similar profiles (Fig. 6) with a downcore increase in all cores, but with pronounced increases associated with landslide-affected sediment in the euxinic and chemocline cores. Total P remains relatively constant in the euxinic (0.13 ± 0.03 wt%) and chemocline (0.12 ± 0.03 wt%) cores (Fig. 6). By contrast, total P concentrations are higher in the upper part of the oxic core and clearly decrease with depth.

To evaluate potential changes in major element compositions due to the landslides, total Fe, Al, Ti, S and P profiles are plotted on a TIC (assuming TIC is present as CaCO_3) and TOC (assuming a formula CH_2O) free basis for the euxinic and chemocline cores in Fig. 7. The data show relatively limited variability in total Fe, Al and Ti for both cores, but in the euxinic core total Fe tends to be slightly lower in landslide-affected sediment, while Al and Ti tend to be slightly higher. These trends likely reflect minor differences in the bulk geochemistry of landslide sediment relative to the normal sediment input. By contrast, total S and P show significant variability on a TOC- and TIC-free basis (Fig. 7). This occurs partly due to dilution of the Fe-sulfides and organic-bound P that form in the water column, by the sediment deposited during landslides, but also reflects biogeochemical cycling during diagenesis, as discussed below.

3.4.2 Iron speciation

In the euxinic core, abundant $\text{Fe(II)}_{\text{unsulf}}$ is present throughout (reaching almost 2 wt%), but the depth profile shows an overall decrease to ~15 cm, and then a subsequent increase below ~20 cm (Fig. 8). In the chemocline and oxic cores, $\text{Fe(II)}_{\text{unsulf}}$ is present at lower concentrations, with an overall slight decrease with depth. With the exception of two isolated samples in the euxinic core, the most reactive iron oxide pool (Fe_{ox1}) is low in all cores (Fig. 8). In contrast, the more crystalline iron (Fe_{ox2}) are more abundant and remain relatively constant with depth (Fig. 8). Fe_{mag} tends to be a minor constituent (Fig. 8), but concentrations are higher from 12.5-20 cm in the euxinic core. Since there is abundant dissolved sulfide at this depth in the euxinic core (Fig. 5), it is unlikely that this is magnetite formed by magnetotactic bacteria (e.g., Karlin et al., 1987), although we cannot rule out the possibility that the magnetite formed *in situ* before sulfidic conditions were re-established after the landslide. Alternatively, the increase in magnetite may be due to increased magnetite concentrations in the landslide sediment, although this is not observed in the lower landslide interval.

Fe_{AVS} is present at relatively low concentrations in all cores, with a general decrease with depth (Fig. 8), presumably due to conversion to pyrite. Fe_{py} is relatively constant at ~1 wt% in the chemocline and oxic cores, although concentrations show a slight increase with depth over the top 12 cm of the oxic core (Fig. 8). In the euxinic core, Fe_{py} shows an overall increase to a depth of ~20 cm, but with a pronounced shift to lower concentrations in association with the most recent landslide. After reaching concentrations of almost 3 wt% below the most recent landslide, Fe_{py} progressively decreases to ~0.1 wt% through the earlier landslide interval (Fig. 8).

3.4.3. Phosphorus speciation

Loosely-bound P (P_{sorb}) concentrations are very low in all three cores (Fig. 9). In the euxinic core, Fe-associated P (P_{Fe}) decreases to a depth of ~15 cm, but then progressively increases below ~18 cm. In the chemocline and oxic cores, P_{Fe} concentration generally decreases with depth, with a particularly strong decrease from relatively high surface concentrations in the oxic core (Fig. 9). P_{Fe} concentration also increases slightly from 15-22 cm depth in the chemocline core. Authigenic carbonate fluorapatite (P_{auth}) is a minor component of all three cores and concentrations remain relatively constant with depth, although there is some suggestion of slightly lower values in landslide intervals (Fig. 9). Detrital P (P_{detr}) varies considerably, particularly across landslide intervals. In the euxinic

core, the two landslide intervals are associated with excursions to much higher concentrations of P_{detr} . Higher concentrations of P_{detr} are also a feature of the landslide interval in the chemocline core (Fig. 9), which presumably reflects differences in the mineralogy of landslide sediment relative to the normal sediment input to the lake. The oxic core displays much less variability in P_{detr} , but there is a clear gradual increase in concentration with depth. Organic-bound P (P_{org}) concentrations decrease with depth in each core, but with excursions to lower values in association with landslide intervals in the euxinic and chemocline cores (Fig. 9).

4. DISCUSSION

4.1. Water column chemistry

Water column data are broadly consistent with previous studies, demonstrating the persistent sulfidic nature of the basin below a depth of ~12 m (Fig. 2). In detail, however, our data highlight temporal variability in the concentrations of different dissolved species. In particular, the concentration of dissolved sulfide at depth ($65 \pm 5 \mu\text{M}$; Fig. 2) is lower than previous reports of 100-300 μM (Halm et al., 2009; Dahl et al., 2010; Canfield et al., 2010). This may be a consequence of lower rates of bacterial sulfate reduction driven by a decrease in the flux of sulfate into the basin (see Boudreau and Westrich, 1984), since concentrations of up to 1.2 mM at depth in the present study (Fig. 2) are significantly lower than previous reports of 1.7-2 mM (Tonolla et al., 1998; Dahl et al., 2010; Canfield et al., 2010). Alternatively, the lower sulfide and sulfate concentrations in the present study may be due to more active mixing between the denser deep lake waters and the upper waters. Similarly, relatively low concentrations of dissolved Fe(II) (~1 μM below the chemocline; Fig. 2) relative to previous reports of up to 3 μM (Tonolla et al., 1998; Halm et al., 2009) may be linked to enhanced water column mixing. Nevertheless, the concentrations of dissolved Fe(II) and sulfide at the time of sampling are in very good agreement with concentrations that would be expected to co-exist according to the solubility of FeS, suggesting that dissolved Fe(II) species are dominated by aqueous FeS clusters (Rickard, 2006).

A pertinent feature of the water column chemistry is the increase in phosphate with depth below the chemocline. Concentrations of up to 2 μM in deeper waters are consistent with previous studies (Tonolla et al., 1998), and the gradual increase observed with depth might be a consequence of release of phosphate either from sinking organic matter during remineralisation via bacterial sulfate reduction, or from the sulfidation of Fe (oxyhydr)oxide

minerals. Alternatively, the phosphate profile may also be generated from the release of phosphate from porewaters, which we consider in more detail below.

4.2. Fe-S systematics

The Fe speciation data show several prominent features of importance to the present study. Firstly, discounting the landslide-affected sediment, there is an overall increase in Fe_{py} to a sediment depth of ~20 cm (Fig. 8). This is consistent with diagenetic pyrite formation augmenting the flux of Fe-sulfide minerals from the water column. The reaction of dissolved sulfide with Fe (oxyhydr)oxide minerals produces mineral surface-associated Fe(II) (i.e., $Fe(II)_{unsulf}$), which subsequently dissolves slowly at the pH of most porewaters (Dos Santos Afonso and Stumm, 1992; Poulton, 2003). The most reactive Fe_{ox1} minerals are initially reduced via this process, and thus this phase is almost entirely consumed in all three cores, whereas the more crystalline Fe (oxyhydr)oxides comprising the Fe_{ox2} pool react more slowly (Canfield, 1989; Canfield et al., 1992; Poulton et al., 2004b) and persist with depth (Fig. 8). After dissolution, Fe(II) can react with dissolved sulfide to form Fe_{AVS} and ultimately pyrite. Thus, the associated decrease in $Fe(II)_{unsulf}$ over the top 15 cm of the euxinic core (and to a lesser extent in the other cores; Fig. 8) is consistent with the progressive formation of pyrite via this process.

By contrast, rapid sedimentation during landslides would dilute the flux of Fe-sulfide minerals forming in the water column, resulting in lower initial concentrations in the deposited sediment. In addition, rapid burial decreases the exposure time of reactive Fe minerals to the highest concentrations of dissolved sulfide, which occurs in the upper portion of sediment (Fig. 5). Dissolved sulfide concentration exerts a primary control on the rate of reductive dissolution of reactive Fe minerals (Canfield et al., 1992; Dos Santos Afonso and Stumm, 1992; Poulton et al., 2003), which would also contribute to the observed decrease in pyrite concentrations in landslide-affected sediment (Fig. 8).

A second prominent feature concerns the persistence of ferric (oxyhydr)oxide mineral phases with depth in all the three cores (dominantly Fe_{ox2} , with minor Fe_{ox1} in some cases). However, the relatively constant Fe_{ox2} depth trends (Fig. 8) are potentially misleading, as the profiles are affected by variable sediment dilution factors arising from the water column formation of TOC, carbonate minerals and pyrite, as well as the landslides. To evaluate whether Fe_{ox2} minerals, which are dominantly introduced to the basin in association with detrital phases, participate in biogeochemical reactions during diagenesis, we plot this phase normalised to Al (as a proxy for the detrital flux) in Fig. 10. These Fe_{ox2}/Al depth profiles

demonstrate that the $\text{Fe}_{\text{ox}2}$ pool is progressively dissolved in both the chemocline and oxic cores, but in particular, there is a major decrease below ~15 cm depth in the euxinic core. The reductive dissolution of $\text{Fe}_{\text{ox}2}$ minerals at depth in the euxinic core would provide the dissolved Fe(II) required to precipitate the high concentrations of pyrite observed at this depth (Fig. 8), and would also source the increase in porewater Fe(II) concentrations observed lower in the core (Fig. 5). In addition, the reduction of $\text{Fe}_{\text{ox}2}$ minerals would account for the progressive increase in $\text{Fe(II)}_{\text{unsulf}}$ below ~15 cm (Fig. 8). Thus, although a proportion of the more crystalline $\text{Fe}_{\text{ox}2}$ minerals persist with depth, these phases are biogeochemically reactive in all cores during diagenesis.

The reduction of crystalline ferric (oxyhydr)oxide minerals deeper in the euxinic core may occur via more than one pathway. Although methane was not measured in our study, anaerobic oxidation of methane has been demonstrated at depths of 16-20 cm in the euxinic sediments of Lake Cadagno (Schubert et al., 2011). Thus AOM using Fe(III) in (oxyhydr)oxide minerals may be responsible for the generation of dissolved Fe(II) (Beal et al., 2009). Alternatively, it is also possible that Fe(II) is sourced from dissimilatory Fe reduction. The production of unsulfidized Fe(II) deeper in the euxinic sediment is a direct consequence of insufficient sulfate (and hence sulfide) to fully sulfidize the Fe_{HR} pool, and we consider the nature of this $\text{Fe(II)}_{\text{unsulf}}$ phase in more detail below.

4.3. Phosphorus cycling

4.3.1. Diagenetic recycling

The dissolved (Fig. 5) and solid phase (Fig. 9) P distributions clearly demonstrate active P cycling in each of the cores. The initial increase in dissolved phosphate observed over the top few cm of each core (Fig. 5), coupled with higher porewater concentrations than in the overlying water column (Fig. 2), likely reflects a balance between release of P from organic matter degradation and Fe (oxyhydr)oxide dissolution during early diagenesis, coupled with diffusive loss of dissolved P to the overlying water column. Although the P_{org} profiles in the euxinic and chemocline cores have clearly been affected by the landslides (Fig. 9), molar $\text{TOC}/\text{P}_{\text{org}}$ ratios (Fig. 11) provide strong evidence for extensive P mobilisation during organic matter degradation. In all cores at depths where the sediment has not been affected by landslides, molar $\text{TOC}/\text{P}_{\text{org}}$ ratios are considerably higher (>600:1) than the Redfield Ratio of 106:1, which is entirely consistent with the preferential recycling of P during bacterial sulfate reduction (Ingall et al., 1993; Slomp et al., 2002, 2004; Jilbert et al., 2011). In landslide-affected intervals, organic matter is more rapidly buried and hence there is less preferential

release of P from organic matter degradation, although even in the most rapidly deposited sediment, $\text{TOC}/\text{P}_{\text{org}}$ ratios are significantly higher than the Redfield Ratio.

4.3.2. Controls on P recycling

The P released from Fe (oxyhydr)oxide reduction and organic matter degradation may either be retained in the sediment as secondary phases, or may be recycled back to the water column (e.g., Ruttenger and Berner, 1993; Ingall and Jahnke, 1994, 1997; Van Cappellen and Ingall, 1994; Slomp et al., 1996b, 2002, 2004). We evaluate these processes by first noting that molar $\text{TOC}/\text{P}_{\text{reactive}}$ ratios are considerably lower than $\text{TOC}/\text{P}_{\text{org}}$ ratios (Fig. 11). These lower $\text{TOC}/\text{P}_{\text{reactive}}$ ratios suggest that some of the recycled organic P is sequestered in authigenic phases, although Fe (oxyhydr)oxide minerals may also contribute an additional source of P to the sediment, consistent with the higher concentrations of P_{Fe} observed in surface sediments (Fig. 9). Nevertheless, despite possible additional P drawdown in association with Fe (oxyhydr)oxides, $\text{TOC}/\text{P}_{\text{reactive}}$ ratios remain well above the Redfield Ratio for sediment intervals not affected by landslides, demonstrating that a significant proportion of the P released during organic matter degradation and Fe (oxyhydr)oxide reduction is recycled back to the water column. This observation is further supported by the relatively low P_{auth} concentrations in all three cores (Fig. 9).

Since the actual fluxes of the different primary reactive P fractions to the sediment are not known, it is not possible to evaluate the relative extent of recycling of different P phases back to the water column. However, close to the sediment water interface, molar $\text{TOC}/\text{P}_{\text{reactive}}$ ratios increase from the oxic core (260:1), through the chemocline core (345:1), to the euxinic core (452:1), consistent with previous studies highlighting the role of water column anoxia, and particularly sulfidic conditions, in enhancing P recycling back to the water column (e.g., Ingall and Jahnke, 1994, 1997; Van Cappellen and Ingall, 1994; Slomp et al., 2002, 2004). A significant flux of P from the sediments under euxinic conditions is supported by the increase in dissolved water column phosphate at depth (Fig. 2). The contrasting behaviour of the P cycle across intervals affected by landslides is also entirely as expected. The rapid burial of sediment would result in a greatly reduced flux of mobilised P back to the water column. Hence, $\text{TOC}/\text{P}_{\text{reactive}}$ ratios are considerably lower across all landslide intervals (Fig. 11).

In terms of retention of dissolved P in the sediment, the carbonate-fluorapatite (P_{aut}) sink is relatively minor (Fig. 9), and much lower than proportions of the total P burial flux typically found in marine sediments deposited beneath oxic bottom waters (~50%; Ruttenger and Berner, 1993). The P_{detr} profiles in the euxinic and chemocline core have been

strongly affected by the deposition of landslide sediment, but in the oxic core there is a minor increase in P_{detr} with depth. This could potentially be due to slight conversion of carbonate fluoroapatite to more crystalline apatite, which would be extracted as P_{detr} . Alternatively, this could be due to a gradual change in the mineralogy of the sediment entering the lake. In either case, this pool does not constitute a major sink for reactive P.

The gradual decrease in dissolved P with depth in the euxinic and chemocline cores does, however, imply the formation of a secondary P phase. In this context, the observed increase in P_{Fe} at depth in the euxinic core (Fig. 9) is particularly significant. The concentration of P_{Fe} begins to increase at a depth of ~20 cm, which is where sulfide concentrations rapidly decrease to low concentrations, and a little below this depth, dissolved Fe(II) increases when dissolved sulfide is completely depleted (Fig. 5). There is no evidence for an increase in reactive Fe (oxyhydr)oxide minerals at this depth (and no evidence for re-adsorption of P; Figs. 8 and 9), and thus this increase in secondary P_{Fe} is unlikely to be due to uptake by ferric oxides (or carbonate minerals; c.f., Kraal et al., 2017). As discussed above, however, there is a clear concomitant increase in $\text{Fe(II)}_{\text{unsulf}}$ with the increase in P_{Fe} . Unlike some of the other solid phase parameters (such as Fe_{py} ; Fig. 8), the increase in $\text{Fe(II)}_{\text{unsulf}}$ does not fluctuate in relation to the landslide-affected sediment. Instead, there is a gradual increase in $\text{Fe(II)}_{\text{unsulf}}$ below ~15 cm depth, indicating that the formation of this phase was not significantly affected by the landslides.

Taken together, the porewater and solid phase geochemical profiles strongly imply the progressive formation of Fe(II) phosphate (vivianite) as porewater sulfate and sulfide become depleted. High concentrations of vivianite are unlikely to occur higher in the core where significant sulfide is present (although vivianite could form in microenvironments, at least as a transient phase; Jilbert and Slomp, 2013), as its formation is suppressed by the formation of FeS (Manning et al., 1994; Reed et al., 2016).

The fine-grained, potentially poorly crystalline nature of vivianite makes direct mineralogical identification problematic at low concentrations in sediments (see Egger et al., 2015). However, geochemical modelling provides support for the formation of vivianite. We initially consider the saturation index (SI) of vivianite and other key diagenetic minerals (pyrite and siderite). The SI of pyrite is high throughout the euxinic core (Fig. 12), but the very low level of sulfide at depth allows dissolved Fe(II) to accumulate in porewaters (Fig. 5). The increased availability of dissolved Fe(II) at depth increases the SI for both siderite and vivianite (Fig. 12), suggesting that both may potentially form. When additionally considered in terms of Eh-pH (Fig. 13), the stability field for pyrite decreases deeper in the sediment, and

at the pH of the euxinic porewaters (~8; Fig. 4), the formation of vivianite is promoted over the formation of siderite.

Our geochemical and modelling data thus support a growing body of evidence for the importance of vivianite as a significant sink for P during sediment diagenesis in a variety of aquatic environments (Rothe et al., 2014; Jilbert and Slomp, 2013; Slomp et al., 2013; Hsu et al., 2014; Egger et al., 2015; O'Connell et al., 2015; Dijkstra et al., 2014; 2016; März et al., 2018). Significantly, however, we provide the first evidence for this process as a major control on the permanent sequestration of P below the sulfate/methane transition in a low sulfate, persistently euxinic water column setting. Egger et al. (2015) found that vivianite formation accounts for 40-50% of total P burial below the sulfate/methane transition zone in sediments deposited beneath the oxic water column of the Bothnian Sea. The total burial flux of P in our euxinic core has been considerably affected by enhanced detrital P inputs from landslide sediment (Fig. 9). However, if we reasonably assume that the majority of P_{Fe} measured at depth in the euxinic core is present as vivianite, then this accounts for up to ~60% of the total reactive P burial flux (i.e., discounting P_{detr}) in euxinic Lake Cadagno sediments. Thus, in low sulfate, euxinic water column settings, vivianite can be a major permanent sink for remobilised phosphorus.

5. SUMMARY AND IMPLICATIONS

We provide the first detailed study of Fe and P cycling in a low sulfate, persistently euxinic setting. Phosphorus recycling to the water column is extensive throughout the basin, but is particularly enhanced beneath the deeper euxinic waters. This is entirely consistent with previous studies of P cycling in anoxic water column settings (e.g., Ingall and Jahnke, 1994, 1997; van Cappellen and Ingall, 1994; Slomp et al., 2002, 2004), but specifically extends this observation to the low sulfate, euxinic settings that were prevalent during Precambrian and Phanerozoic episodes of water column euxinia. Phosphorus recycling significantly diminishes the overall P burial efficiency (Ingall and Jahnke, 1994; 1997), thus altering the total P content of the sediment, as well as TOC/ P_{org} ratios, providing support for the suggestion (Poulton, 2017) that the total P content of ancient euxinic shales is unlikely to track water column P concentrations (c.f., Reinhard et al., 2017).

As previously suggested, the recycling of P back to the water column in ancient euxinic settings would promote a positive productivity feedback, significantly enhancing organic carbon burial (Ingall and Jahnke, 1994; 1997; Van Cappellen and Ingall, 1994) and hence oxygen production. However, our data also suggest that the flux of recycled P to the water

column in ancient euxinic settings would have been modulated by the formation of authigenic Fe(II) phosphate minerals. This would specifically occur because, as demonstrated in Lake Cadagno, the low-sulfate concentrations result in sulfide depletion (through precipitation as pyrite), and hence vivianite precipitation, relatively close to the sediment-water interface. This scenario is very different to other modern, high sulfate euxinic settings, where in shallow sediments vivianite has been found forming in microenvironments within sediments that still contain significant dissolved sulfide (Jilbert and Slomp, 2013), but only as a transient phase (Kraal et al., 2017) that does not significantly impact P cycling (Reed et al., 2016). Thus, the recycling flux of P to the water column from high sulfate, euxinic settings is unlikely to be significantly modified by the precipitation of vivianite.

More often, vivianite formation has been observed at significant depth in the sediment profile, where internal P recycling below the sulfate-methane transition promotes vivianite formation at depths of several metres (e.g., Dijkstra et al., 2016; 2018; März et al., 2018), with no net effect on P recycling from the sediment. We additionally note that in addition to requiring dissolved P, the formation of Fe(II) phosphate requires that unsulfidized Fe_{HR} minerals persist beneath the sulfate/methane transition zone. This persistence of unsulfidized Fe_{HR} minerals would also be enhanced in low sulfate, euxinic settings, compared to high sulfate, euxinic settings, due to the decreased average exposure time of Fe (oxyhydr)oxide minerals to high concentrations of dissolved sulfide (see Poulton et al., 2004a). In this context, we note that studies of ancient marine settings have demonstrated that ~30% of the Fe_{HR} pool commonly remains unsulfidized under low sulfate, euxinic water column conditions (März et al., 2008b). Thus, ancient euxinic settings commonly contained sufficient unsulfidized Fe_{HR} to promote vivianite formation beneath a shallow sulfate/methane transition zone.

The relative extent of water column P regeneration under euxinic conditions through Earth's history can be considered to be sulfate-dependent, since on a global scale, sulfate concentration will (at least partly) determine the depth in the sediment at which Fe(II) phosphate becomes a significant sink for remobilised P. In other words, on a global scale, low sulfate promotes vivianite formation closer to the sediment-water interface, due to the more rapid consumption of all of the dissolved sulfate and sulfide during early diagenesis. Enhanced vivianite formation closer to the sediment-water interface under low sulfate conditions would decrease the flux of P back to the water column. Thus, as sulfate concentrations increased from the low micromolar range typical of the early Archean (Habicht et al., 2002; Crowe et al., 2014), through the low millimolar range of the later

Proterozoic (Kah et al., 2004; Guilbaud et al., 2015), to the moderate millimolar range of many Phanerozoic euxinic episodes (e.g., Adams et al., 2010; Newton et al., 2011; Song et al., 2013; Poulton et al., 2015), the significance of the Fe(II) phosphate trap for remobilised P under euxinic conditions likely progressively diminished. As such, the formation of vivianite would not be expected to exert such a strong control on P recycling under the higher sulfate concentrations typical of modern euxinic marine settings. As a natural extension of these observations, our data suggest that P recycling likely maintained mid-Proterozoic, shallow marine phosphate concentrations at moderate, rather than very low (c.f., Reinhard et al., 2017) levels, under the widespread euxinic conditions envisaged for such settings (e.g., Canfield, 1998; Scott et al., 2008; Poulton et al., 2010; Poulton and Canfield, 2011; Kendall et al., 2011), with significant implications for organic carbon production and burial, and hence the production of atmospheric oxygen.

ACKNOWLEDGEMENTS

This work was supported by a University of Leeds (School of Earth and Environment) research training grant to YX. SWP acknowledges support from a Royal Society Wolfson Research Merit Award and a Leverhulme Trust Fellowship. DEC acknowledges generous support from the Villum Foundation and from the University of Southern Denmark. We are grateful to Christian März, Peter Kraal, two anonymous reviewers and editor Sabine Kasten for insightful comments that helped improve the final manuscript.

APPENDIX A. SUPPLEMENTARY DATA

Supplementary data associated with this article can be found in the online version.

REFERENCES

- Adams D. D., Hurtgen M. T. and Sageman B. B. (2010) Volcanic triggering of a biogeochemical cascade during Oceanic Anoxic Event 2. *Nat. Geosci.* **3**, 201-204.
- Anbar A. D. and Knoll A. H. (2002) Proterozoic ocean chemistry and evolution: A bioinorganic bridge? *Science* **297**, 1137-1142.
- Anschutz P., Zhong S., Sundby B., Mucci A. and Gobeil C. (1998) Burial efficiency of phosphorus and the geochemistry of iron in continental margin sediments. *Limnol. Oceanogr.* **43**, 53-64.
- Appelo C. A. J., Parkhurst D. L. and Post V. E. A. (2014) Equations for calculating hydrogeochemical reactions of minerals and gases such as CO₂ at high pressures and temperatures. *Geochim. Cosmochim. Acta* **125**, 49-67.
- Beal, E. J., House, C. H. and Orphan, V. J. (2009) Manganese- and Iron-Dependent Marine Methane Oxidation. *Science* **325**, 184-187.
- Berner R. A. (1990) Diagenesis of phosphorus in sediments from non-upwelling areas. In Burnett, W.C., Riggs, S.R. (Eds.), *Phosphate Deposits of the World Volume 3: Neogene to Modern Phosphorites*. Cambridge University Press, p27-32.
- Birch L., Hanselmann K. W. and Bachofen R. (1996) Heavy metal conservation in Lake Cadagno sediments: Historical records of anthropogenic emissions in a meromictic alpine lake. *Water Res.* **30**, 679-687.
- Bjerrum C. J. and Canfield D. E. (2002) Ocean productivity before about 1.9 Gyr ago limited by phosphorus adsorption onto iron oxides. *Nature* **417**, 159-162.
- Boudreau B. P. and Westrich J. T. (1984) The dependence of bacterial sulfate reduction on sulfate concentration in marine sediments. *Geochim. Cosmochim. Acta* **48**, 2503-2516.
- Canfield D. E. (1989) Reactive iron in marine sediments. *Geochim. Cosmochim. Acta* **53**, 619-632.
- Canfield D. E. (1998) A new model for Proterozoic ocean chemistry. *Nature* **396**, 450-453.
- Canfield D. E. (2005) The early history of atmospheric oxygen: Homage to Robert M. Garrels. *Annu. Rev. of Earth Planet. Sci.* **33**, 1-36.
- Canfield D. E., Raiswell R., Westrich J. T., Reaves C. M. and Berner R. A. (1986) The use of chromium reduction in the analysis of reduced inorganic sulfur in sediments and shales. *Chem. Geol.* **54**, 149-155.
- Canfield D. E., Raiswell R. and Bottrell S. (1992) The reactivity of sedimentary iron minerals towards sulfide. *Amer. J. Sci.* **292**, 659-683.

- Canfield D. E., Rösing M. T. and Bjerrum C. (2006) Early anaerobic metabolisms. *Phil. Trans. Roy. Soc. B* **361**, 1819-1836.
- Canfield D. E., Poulton S. W., Knoll A. H., Narbonne G. M., Ross G., Goldberg T. and Strauss H. (2008) Ferruginous conditions dominated Later Neoproterozoic deep-water chemistry. *Science* **321**, 949-952.
- Canfield D. E., Farquhar J. and Zerkle A. L. (2010) High isotope fractionations during sulfate reduction in a low-sulfate euxinic ocean analog. *Geology* **38**, 415-418.
- Cline J. D. (1969) Spectrophotometric determination of hydrogen sulfide in natural waters. *Limnol. Oceanogr.* **14**, 454-458.
- Codispoti L. A., Friederich G. E., Murray J. W. and Sakamoto C. M. (1991) Chemical variability in the Black Sea: implications of continuous vertical profiles that penetrated the oxic/anoxic interface. *Deep-Sea Res.* **38**, 691-710.
- Crowe S. A., Paris G., Katsev S., Jones C., Kim S., Zerkle A. L., Nomosatryo S., Fowle D. A., Adkins J. F., Sessions A. L., Farquhar J. and Canfield D. E. (2014) Sulfate was a trace constituent of Archean. *Science* **346**, 735-739.
- Dahl T. W., Anbar A. D., Gordon G. W., Rosing M. T., Frei R. and Canfield D. E. (2010) The behavior of molybdenum and its isotopes across the chemocline and in the sediments of sulfidic Lake Cadagno, Switzerland. *Geochim. Cosmochim. Acta* **74**, 144-163.
- Daines S. J., Mills B. J. W. and Lenton T. M. (2016) Atmospheric oxygen regulation at low Proterozoic levels by incomplete oxidative weathering of sedimentary organic carbon. *Nat. Commun.* **8**, 1-11.
- Del Don C., Hanselmann K. W., Peduzzi R. and Bachofen R. (1998) Orographical and geochemical description of the meromictic Alpine Lake Cadagno. *Documenta Ist. Ital. Idrobiol.* **63**, 5-9.
- Del Don C., Hanselmann K. W., Peduzzi R. and Bachofen R. (2001) The meromictic alpine Lake Cadagno: orographical and biogeochemical description. *Aquat. Sci.* **63**, 70-90.
- Dellwig O., Leipe T., März C., Glockzin M., Pollehne F., Schnetger B., Yakushev E. V., Boettcher M. E. and Brumsack H. (2010) A new particulate Mn-Fe-P-shuttle at the redoxcline of anoxic basins. *Geochim. Cosmochim. Acta* **74**, 7100-7115.
- Dijkstra N., Kraal P., Kuypers M. M. M., Schnetger B. and Slomp C. P. (2014) Are iron-phosphate minerals a sink for phosphorus in anoxic Black Sea sediments? *PLoS ONE* **9**, e101139.
- Dijkstra N., Slomp C. P., Behrends T. and Expedition 347 Scientists (2016) Vivianite is a key sink for phosphorus in sediments of the Landsort Deep, an intermittently anoxic deep basin in the Baltic Sea. *Chem. Geol.* **438**, 58-72.

- Dijkstra N., Hagens, M., Egger, M. and Slomp, C.P. (2018) Post-depositional formation of vivianite-type minerals alters sediment phosphorus records. *Biogeosci.* **15**, 861-883.
- Dos Santos Afonso M. and Stumm W. (1992) Reductive dissolution of iron (III) (hydr)oxides by hydrogen sulfide. *Langmuir* **8**, 1671-1675.
- Egger M., Jilbert T., Behrends T., Rivard C. and Slomp C. P. (2015) Vivianite is a major sink for phosphorus in methanogenic coastal surface sediments. *Geochim. Cosmochim. Acta* **169**, 217-235.
- Fennel K., Follows M. and Falkowski P. G. (2005) The coevolution of the nitrogen, carbon and oxygen cycles in the Proterozoic ocean. *Am. J. Sci.* **305**, 526-545.
- Fossing H. and Jørgensen B. B. (1989) Measurement of bacterial sulfate reduction in sediments: Evaluation of a single-step chromium reduction method. *Biogeochemistry* **8**, 205-222.
- Froelich P. N., Arthur M. A., Burnett W. C., Deakin M., Hensley V., Jahnke R., Kaul L., Kim K.-H., Roe K., Soutar A. and Vathakanon C. (1988) Early diagenesis of organic matter in Peru continental margin sediments: phosphorite precipitation. *Mar. Geol.* **80**, 309-343.
- Gill B. C., Lyons T. W., Young S. A., Kump L. R., Knoll A. H. and Saltzman M. R. (2011) Geochemical evidence for widespread euxinia in the Later Cambrian ocean. *Nature* **469**, 80-83.
- Godfrey L. V., Poulton S. W., Bebout G. E. and Fralick P. W. (2013) Stability of the nitrogen cycle during development of sulfidic water in the redox-stratified late Paleoproterozoic ocean. *Geology* **41**, 655-658.
- Goldberg T., Archer C., Vance D., Thamdrup B., McAnena A. and Poulton S. W. (2012) Controls on Mo isotope fractionations in a Mn-rich anoxic marine sediment, Gullmar Fjord, Sweden. *Chem. Geol.* **296-297**, 73-82.
- Guilbaud R., Poulton S. W., Butterfield N. J., Zhu M. and Shields-Zhou G. A. (2015) A global transition to ferruginous conditions in the early Neoproterozoic oceans. *Nat. Geosci.* **8**, 466-470.
- Gregersen L. H., Habicht K. S., Peduzzi S., Tonolla M., Canfield D. E., Miller M., Cox R. P. and Frigaard N.-U. (2009) Dominance of a clonal green sulfur bacterial population in a stratified lake. *FEMS Microbiol. Ecol.* **70**, 30-41.
- Habicht K. S., Gade M., Thamdrup B., Berg P. and Canfield D. E. (2002) Calibration of Sulfate Levels in the Archean Ocean. *Science* **298**, 2372-2374.
- Hall P. O. J. and Aller R. C. (1992) Rapid, small-volume flow injection analysis for CO₂ and NH₄⁺ in marine and freshwaters. *Limnol. Oceanogr.* **37**, 1113-1119.

- Halm H., Musat N., Lam P., Langlois R., Musat F., Peduzzi S., Lavik G., Schubert C. J., Sinha B., LaRoche J. and Kuypers M. M. (2009) Co-occurrence of denitrification and nitrogen fixation in a meromictic lake, Lake Cadagno (Switzerland), *Environ. Microbiol.* **11**, 1945-1958.
- Hammarlund E. U., Dahl T. W., Harper D. A. T., Bond D. P. G., Nielsen A. T., Bjerrum C. J., Schovsbo N. H., Schönlaub H., Zalasiewicz J. A. and Canfield D. E. (2012) A sulfidic driver for the end-Ordovician mass extinction. *Earth Planet. Sci. Lett.* **331-332**, 128-139.
- Howarth R. (1988) Nutrient limitation of net primary production in marine ecosystems. *Ann. Rev. Ecol.* **19**, 89-110.
- Hsu T., Jiang W. and Wang Y. (2014) Authigenesis of vivianite as influenced by methane-induced sulfidization in cold-seep sediments off southwestern Taiwan. *J. Asian Earth Sci.* **89**, 88-97.
- Ingall E. D. and Jahnke R. (1994) Evidence for enhanced phosphorus regeneration from marine sediments overlain by oxygen depleted waters. *Geochim. Cosmochim. Acta* **58**, 2571-2575.
- Ingall E. D. and Jahnke R. (1997) Influence of water-column anoxia on the elemental fractionation of carbon and phosphorus during sediment diagenesis. *Mar. Geol.* **139**, 219-229.
- Ingall E. D., Bustin R. M. and van Cappellen P. (1993) Influence of water column anoxia on the burial and preservation of carbon and phosphorus in marine shales. *Geochim. Cosmochim. Acta* **57**, 303-316.
- Jenkyns H. C. (2010) Geochemistry of oceanic anoxic events. *Geochem. Geophys. Geosyst.* **11**, doi: 10.1029/2009GC002788.
- Jilbert T. and Slomp C. P. (2013) Iron and manganese shuttles control the formation of authigenic phosphorus minerals in the euxinic basins of the Baltic Sea. *Geochim. Cosmochim. Acta* **107**, 155-169.
- Jilbert T., Slomp C. P., Gustafsson B. G. and Boer W. (2011) Beyond the Fe-P-redox connection: preferential regeneration of phosphorus from organic matter as a key control on Baltic Sea nutrient cycles. *Biogeosciences* **8**, 1699-1720.
- Johnston D. T., Wolfe-Simon F., Pearson A. and Knoll A. H. (2009) Proterozoic Ocean Chemistry and Evolution: A Bioinorganic Bridge? *Proc. Natl. Acad. Sci. U.S.A.* **106**, 16925-16929.
- Johnston D. T., Poulton S. W., Dehler C., Porter S., Husson J., Canfield D. E. and Knoll A. H. (2010) An emerging picture of Neoproterozoic ocean chemistry: Insights from the Chuar Group, Grand Canyon, USA. *Earth Planet. Sci. Lett.* **290**, 64-73.
- Jones C., Nomosatryo S., Crowe S. A., Bjerrum C. J. and Canfield D. E. (2015) Iron oxides, divalent cations, silica, and the early earth phosphorus crisis. *Geology* **43**, 135-138.

- Joshi, S. R., Kukkadapu, R. K., Burdige, D., Bowden, M., Sparks, D. L. and Jaisi, D. P. (2015) Organic matter remineralization predominates phosphorus cycling in the mid-Bay sediment in the Chesapeake Bay. *Environ. Sci. Technol.* **49**, 5887-5896.
- Kah L. C., Lyons T. W. and Frank T. D. (2004) Low marine sulphate and protracted oxygenation of the Proterozoic biosphere. *Nature* **431**, 834-838.
- Karlin R., Lyle M. and Heath C. R. (1987) Authigenic magnetite formation in suboxic marine sediments. *Nature* **326**, 490-493.
- Kendall B., Reinhard C. T., Lyons T. W., Kaufman A. J., Poulton S. W. and Anbar A. D. (2010) Pervasive oxygenation along late Archaean ocean margins. *Nat. Geosci.* **3**, 647-652.
- Knoll-Heitz F. (1991) Piora-Konzept für die Erhaltung einer Landschaft (Piora-a concept for the preservation of a landscape). WWF Sezione Svizzera Italiana, St Gallen, Switzerland.
- Koehler M. C., Stüeken E. E., Kipp M. A., Buick R. and Knoll A. H. (2017) Spatial and temporal trends in Precambrian nitrogen cycling: a Mesoproterozoic offshore nitrate minimum. *Geochim. Cosmochim. Acta* **198**, 315-337.
- Konhauser K. O., Newman D. K. and Kappler A. (2005) The potential significance of microbial Fe(III) reduction during deposition of Precambrian banded iron formations. *Geobiology* **3**, 167-177.
- Konhauser K. O., Lalonde S. V., Amskold L. and Holland H. D. (2007) Was there really an Archean phosphate crisis? *Science* **315**, 1234.
- Koroleff F. (1976) Determination of phosphorus. In *Methods of seawater analysis*, 2nd ed. (eds. K. Grasshoff et al.). Verlag Chemie, Weinheim, pp. 117-156.
- Kraal P., Dijkstra N., Behrends T. and Slomp C. P. (2017) Phosphorus burial in sediments of the sulfidic deep Black Sea: Key roles for adsorption by calcium carbonate and apatite authigenesis. *Geochim. Cosmochim. Acta* **204**, 140-158.
- Krige L. J. (1917) Petrographische Untersuchungen im Val Piora und Umgebung. *Eclogae Geol. Helv.* **14**, 519-654.
- Krom M. D. and Berner R. A. (1980) Adsorption of phosphate in anoxic marine sediments. *Limnol. Oceanogr.* **25**, 797-806.
- Krom M. D. and Berner R. A. (1981) The diagenesis of phosphorus in a nearshore marine sediment. *Geochim. Cosmochim. Acta* **45**, 207-216.
- Laliberté M. (2009) A model for calculating the heat capacity of aqueous solutions, with updated density and viscosity data. *J. Chem. Eng. Data.* **54**, 1725-1760.
- Li C., Love G. D., Lyons T. W., Fike D. A., Sessions A. L. and Chu X. (2010) A Stratified Redox Model for the Ediacaran Ocean. *Science* **328**, 80-83.

- Li C., Love G. D., Lyons T. W., Scott C. T., Feng L., Huang J., Chang H., Zhang Q. and Chu X. (2012) Evidence for a redox stratified Cryogenian marine basin, Datangpo Formation, South China. *Earth Planet. Sci. Lett.* **331-332**, 246-256.
- Lyons T. W., Reinhard C. T. and Planavsky N. J. (2014) The rise of oxygen in Earth's early ocean and atmosphere. *Nature* **506**, 307-315.
- März C., Hoffmann J., Bleil U., de Lange G. J. and Kasten S. (2008a) Diagenetic changes of magnetic and geochemical signals by anaerobic methane oxidation in sediments of the Zambezi deep-sea fan (SW Indian Ocean). *Mar. Geol.* **255**, 118-130.
- März C., Poulton S. W., Beckmann B., Küster K., Wagner T. and Kasten S. (2008b) Redox sensitivity of P cycling during marine black shale formation: Dynamics of sulfidic and anoxic, non-sulfidic bottom waters. *Geochim. Cosmochim. Acta* **72**, 3703-3717.
- März C., Riedinger N., Sena C., and Kasten S. (2018) Phosphorus dynamics around the sulphate-methane transition in continental margin sediments: Authigenic apatite and Fe(II) phosphates. *Marine Geology* **404**, 84-96.
- Madsen H. E. L. and Hansen H. C. B. (2014) Kinetics of crystal growth of vivianite, $\text{Fe}_3(\text{PO}_4)_2 \cdot 8\text{H}_2\text{O}$, from solution at 25, 35 and 45°C. *J. Cryst. Growth* **401**, 82-86.
- Manning P. G., Murphy T. P. and Prepas E. E. (1994) Forms of iron and the bioavailability of phosphorus in eutrophic Amisk Lake, Alberta. *Can. Mineral.* **32**, 459-468.
- Michiels C. C., Darchambeau F., Roland F. A. E., Morana C., Llíros M., García-Armisen T., Thamdrup B., Borges A. V., Canfield D. E., Servais P., Descy J. and Crowe S. A. (2017) Iron-dependent nitrogen cycling in a ferruginous lake and the nutrient status of Proterozoic oceans. *Nat. Geosci.* **10**, 217-221.
- Mort H. P., Adatte T., Föllmi K., Keller G., Steinmann P., Matera V., Berner Z. and Stüben D. (2007) Phosphorus and the roles of productivity and nutrient recycling during oceanic anoxic event 2. *Geology* **35**, 483-486.
- Newton R. J., Reeves E. P., Kafousia N., Wignall P. B., Bottrell S. and Sha J. (2011) Low marine sulfate concentrations and the isolation of the European epicontinental sea during the Early Jurassic. *Geology* **39**, 7-10.
- O'Connell D. W., Jensen M. M., Jakobsen R., Thamdrup B., Andersen T. J., Kovacs A. and Hansen H. C. B. (2015) Vivianite formation and its role in phosphorus retention in Lake Ørn, Denmark. *Chem. Geol.* **409**, 42-53.
- Och L. M., Cremonese L., Shields-Zhou G. A., Poulton S. W., Struck U., Ling H., Li D., Chen X., Manning C., Thirlwall M., Strauss H. and Zhu M. (2016) Palaeoceanographic controls on spatial redox distribution over the Yangtze Platform during the Ediacaran–Cambrian transition. *Sedimentology* **63**, 378-410.

Peiffer S., Dos Santos Afonso M., Wehrli B. and Gaechter R. (1992) Kinetics and mechanism of the reaction of H₂S with lepidocrocite. *Environ. Sci. Technol.* **26**, 2408-2413.

Poulton S. W. (2003) Sulfide oxidation and iron dissolution kinetics during the reaction of dissolved sulfide with ferrihydrite. *Chem. Geol.* **202**, 79-94.

Poulton S. W. (2017) Early phosphorus redigested. *Nat. Geosci.* **10**, 75-76.

Poulton S. W. and Canfield D. E. (2005) Development of a sequential extraction procedure for iron: implications for iron partitioning in continentally derived particulates. *Chem. Geol.* **214**, 209-221.

Poulton S. W. and Canfield D. E. (2011) Ferruginous conditions: A dominant feature of the ocean through Earth's history. *Elements* **7**, 107-112.

Poulton S. W., Fralick P. W. and Canfield D. E. (2004a) The transition to a sulphidic ocean ~ 1.84 billion years ago. *Nature* **431**, 173-177.

Poulton S. W., Krom M. D. and Raiswell R. (2004b) A revised scheme for the reactivity of iron (oxyhydr)oxide minerals towards dissolved sulfide. *Geochim. Cosmochim. Acta* **68**, 3703-3715.

Poulton S. W., Fralick P. W. and Canfield D. E. (2010) Spatial variability in oceanic redox structure 1.8 billion years ago. *Nat. Geosci.* **3**, 486-490.

Poulton S. W., Henkel S., März C., Urquhart H., Flögel S., Kasten S., Sinninghe Damsté J. S. and Wagner T. (2015) A continental-weathering control on orbitally driven redox-nutrient cycling during Cretaceous Oceanic Anoxic Event 2. *Geology* **43**, 963-966.

Planavsky N. J., Rouxel O. J., Bekker A., Lalonde S. V., Konhauser K. O., Reinhard C. T. and Lyons T. W. (2010) The evolution of the marine phosphate reservoir. *Nature* **467**, 1088-1090.

Planavsky N. J., Reinhard C. T., Wang X., Thomson D., McGoldrick P., Rainbird R. H., Johnson T., Fischer W. W. and Lyons T. W. (2014) Low Mid-Proterozoic atmospheric oxygen levels and the delayed rise of animals. *Science* **346**, 635-638.

Pyzik A. J. and Sommer S. E. (1981) Sedimentary iron monosulfides: Kinetics and mechanism of formation. *Geochim. Cosmochim. Acta* **45**, 687-698.

Raiswell R. and Canfield D. E. (1998) Sources of iron for pyrite formation in marine sediments. *Am. J. Sci.* **298**, 219-245.

Reed D. C., Gustafsson B. G. and Slomp C. P. (2016) Shelf-to-basin iron shuttling enhances vivianite formation in deep Baltic Sea sediments. *Earth Planet. Sci. Lett.* **434**, 241-251.

Reinhard C. T., Raiswell R., Scott C., Anbar A. D. and Lyons T. W. (2009) A Late Archean sulfidic sea stimulated by early oxidative weathering of the continents. *Science* **326**, 713-716.

Reinhard C. T., Planavsky N. J., Gill B. C., Ozaki K., Robbins L. J., Lyons T. W., Fischer W. W., Wang C., Cole D. B. and Konhauser K. O. (2017) Evolution of the global phosphorus cycle. *Nature* **541**, 386-401.

Rickard D. (2006) The solubility of FeS. *Geochim. Cosmochim. Acta* **70**, 5779-5789.

Riedinger N., Formolo M. J., Lyons T. W., Henkel S., Beck A. and Kasten S. (2014) An inorganic geochemical argument for coupled anaerobic oxidation of methane and iron reduction in marine sediments. *Geobiology* **12**, 172-181.

Rothe M., Frederichs T., Eder M., Kleeberg A. and Hupfer M. (2014) Evidence for vivianite formation and its contribution to long-term phosphorus retention in a recent lake sediment: a novel analytical approach. *Biogeosciences* **11**, 5169-5180.

Ruttenberg, K. C. (1992) Development of a sequential extraction method for different form of phosphorus in marine sediments. *Limnol. Oceanogr.* **37**, 1460-1482.

Ruttenberg K. C. and Berner R. (1993) Authigenic apatite formation and burial in sediments from non-upwelling, continental margin environments. *Geochim. Cosmochim. Acta* **57**, 991-1007.

Sahoo S. K., Planavsky N. J., Kendall B., Wang X., Shi X., Scott C., Anbar A. D., Lyons T. W. and Jiang G. (2012) Ocean oxygenation in the wake of the Marinoan glaciation. *Nature* **489**, 546-549.

Schubert C. J., Vazquez F., Losekann-Behrens T., Knittel K., Tonolla M. and Boetius A. (2011) Evidence for anaerobic oxidation of methane in sediments of a freshwater system (Lago di Cadagno). *FEMS Microbiol. Ecol.* **76**, 26-38.

Scott C.T., Lyons T. W., Bekker A., Shen Y., Poulton S. W., Chu X. and Anbar A. D. (2008) Tracing the stepwise oxygenation of the Proterozoic ocean. *Nature* **452**, 456-459.

Scott C. T., Bekker A., Reinhard C. T., Schmetger B., Krapež B., Rumble III D. and Lyons T. W. (2011) Late Archean euxinic conditions before the rise of atmospheric oxygen. *Geology* **39**, 119-122.

Slomp C. P. and van Raaphorst W. (1993) Phosphate adsorption in oxidized marine sediments. *Chem. Geol.* **107**, 477-480.

Slomp C. P., Epping E. H. G., Helder W. and van Raaphorst W. (1996a) A key role for iron-bound phosphorus in authigenic apatite formation in North Atlantic continental platform sediments. *J. Mar. Res.* **54**, 1179-1205.

Slomp C. P., Van der Gaast S. J. and van Raaphorst W. (1996b) Phosphorus binding by poorly crystalline iron oxides in North Sea sediments. *Mar. Chem.* **52**, 55-73.

Slomp C. P., Thompson J. and de Lange G. J. (2002) Enhanced regeneration of phosphorus during formation of the most recent eastern Mediterranean sapropel (S1). *Geochim. Cosmochim. Acta* **66**, 1171-1184.

Slomp C. P., Thomson J. and de Lange G. J. (2004) Controls on phosphorus regeneration and burial during formation of eastern Mediterranean sapropels. *Mar. Geol.* **203**, 141-159.

Slomp C. P., Mort H. P., Jilbert T., Reed D. C., Gustafsson B. G. and Wolthers M. (2013) Coupled dynamics of iron and phosphorus in sediments of an oligotrophic coastal basin and the impact of anaerobic oxidation of methane. *PLoS ONE* **8**, e62386.

Song H., Tong J., Algeo T. J., Song H., Qiu H., Zhu Y., Tian L., Bates S., Lyons T. W., Luo G. and Kump L. R. (2013) Early Triassic seawater sulfate drawdown. *Geochim. Cosmochim. Acta* **128**, 95-113.

Sperling E. A., Wolock C. J., Morgan A. S., Gill B. C., Kunzmann M., Halverson G. P., Macdonald F. A., Knoll A. H. and Johnston D. T. (2015) Statistical analysis of iron geochemical data suggests limited late Proterozoic oxygenation. *Nature* **523**, 451-454.

Steenbergh A. K., Bodelier P. L. E., Hoogveld H. L., Slomp C. P. and Laanbroek H. J. (2011) Phosphatases relieve carbon limitation of microbial activity in Baltic Sea sediments along a redox-gradient. *Limnol. Oceanogr.* **56**, 2018-2026.

Stookey L. L. (1970) Ferrozine-A new spectrophotometric reagent for iron. *Anal. Chem.* **42**, 779-781.

Stüeken E. E. (2013) A test of the nitrogen-limitation hypothesis for retarded eukaryote radiation: nitrogen isotopes across a Mesoproterozoic basinal profile. *Geochim. Cosmochim. Acta* **120**, 121-139.

Thauer R. K. and Shima S. (2008) Methane as fuel for anaerobic microorganisms. *Ann. N. Y. Acad. Sci.* **1125**, 158-170.

Thomson D., Rainbird R. H., Planavsky N., Lyons T. W. and Bekker A. (2015) Chemostratigraphy of the Shaler Supergroup, Victoria Island, NW Canada: A record of ocean composition prior to the Cryogenian glaciations. *Precamb. Res.* **263**, 232-245.

Tonolla M., Demarta A. and Peduzzi R. (1998) The chemistry of Lake Cadagno. In *Lake Cadagno: A meromictic alpine lake*. (eds. Peduzzi R. et al.). Consiglio nazionale delle ricerche, Istituto italiano di idrobiologia, Verbania Pallanza, pp. 11-17

Tonolla M., Demarta A., Peduzzi R. and Hahn D. (1999) *In situ* analysis of phototrophic sulfur bacteria in the chemocline of meromictic Lake Cadagno (Switzerland). *Appl. Environ. Microbiol.* **65**, 1325-1330.

Tyrrell T. (1999) The relative influences of nitrogen and phosphorus on oceanic primary production. *Nature* **400**, 525-531.

Van Cappellen P. and Ingall E. D. (1994) Benthic phosphorus regeneration, net primary production, and ocean anoxia: A model of the coupled marine biogeochemical cycles of carbon and phosphorus. *Paleoceanography* **9**, 677-692.

Viollier E., Hunter K., Roychoudhury A. N. and van Cappellen P. (2000) The ferrozine method revisited: Fe(II)/Fe(III) determination in natural waters. *Appl. Geochem.* **15**, 785-790.

Wignall P. B. and Twitchett R. J. (1996) Oceanic anoxia and the End Permian mass extinction. *Science* **272**, 1155-1158.

Wignall P. B., Bond D. P. G., Kuwahara K., Kakuwa Y., Newton R. J. and Poulton S. W. (2010) An 80 million year oceanic redox history from Permian to Jurassic pelagic sediments of the Mino-Tamba terrane, SW Japan, and the origin of four mass extinctions. *Glob. Planet. Chang.* **71**, 109-123.

Wirth S. B., Gilli A., Niemann H., Dahl T. W., Ravasi D., Sax N., Hamann Y., Peduzzi R., Peduzzi S., Tonolla, M., Lehmann, M. F. and Anselmetti F. S. (2013) Combining sedimentological, trace metal (Mn, Mo) and molecular evidence for reconstructing past water-column redox conditions: The example of meromictic Lake Cadagno (Swiss Alps). *Geochim. Cosmochim. Acta* **120**, 220-238.

Yakushev E. V., Chasovnikov V. K., Murray J. W., Pakhomova S. V., Podymov O. I. and Stunzhas P. A. (2008) Vertical hydrochemical Structure of the Black Sea. *Handbook Environ. Chem.* **5**, 277-307.

Zegeye A., Bonneville S., Benning L. G., Sturm A., Fowle D. A., Jones C., Canfield D. E., Ruby C., MacLean L. C., Nomosatryo S., Crowe S. A. and Poulton S. W. (2012) Green rust formation controls nutrient availability in a ferruginous water column. *Geology* **40**, 599-602.

Zerkle A. L., House C., Cox R. and Canfield D. (2006) Metal limitation of cyanobacterial N₂ fixation and implications for the Precambrian nitrogen cycle. *Geobiology* **4**, 285-297.

Zhang Y., Jacob D. J., Horowitz H., M., Chen L., Amos H. M., Krabbenhoft D. P., Slemr F., St. Louis V. L. and Sunderland E. M. (2016) Observed decrease in atmospheric mercury explained by global decline in anthropogenic emissions. *Proc. Natl. Acad. Sci. U.S.A.* **113**, 526-531.

Figure Captions

Fig. 1. Geographical map and bathymetric map of Lake Cadagno, Switzerland (after Wirth et al., 2013; Tonolla et al., 1998). Circles indicate the three sediment core locations, and the squares indicates the position of the subaquatic springs.

Fig. 2. Vertical distribution of dissolved O_2 , SO_4^{2-} , Fe^{2+} , sulfide, and PO_4^{3-} in the water column of Lake Cadagno. The O_2 profile is from Canfield et al. (2010).

Fig. 3. Water content profiles; a) euxinic core; b) chemocline core. Dashed lines indicate general depth trends.

Fig. 4. Dissolved inorganic carbon (DIC) and pH in the euxinic core porewaters.

Fig. 5. Porewater profiles for dissolved Fe^{2+} , PO_4^{3-} , sulfide and SO_4^{2-} ; a) sulfide and SO_4^{2-} in the euxinic core; b) Fe^{2+} and PO_4^{3-} in the euxinic core; c) sulfide and SO_4^{2-} in the chemocline core; d) Fe^{2+} and PO_4^{3-} in the chemocline core; e) sulfide and SO_4^{2-} in the oxic core; f) Fe^{2+} and PO_4^{3-} in the oxic core.

Fig. 6. Profiles of TIC, TOC, TS, Fe, Al, Ti and P for the three sediment cores. Grey shading marks landslide intervals.

Fig. 7. Profiles of total Fe, Al, Ti, S and P on a TOC-free and TIC-free basis for the euxinic and chemocline cores. Grey shading marks landslide intervals.

Fig 8. Iron speciation profiles in the three sediment cores. Grey shading marks landslide intervals.

Fig 9. P speciation profiles for the three sediment cores. Grey shading marks landslide intervals.

Fig. 10. Fe_{ox2}/Al depth profiles for the three sediment cores; a) euxinic core; b) chemocline core; c) oxic core. Grey shading marks landslide intervals.

Fig. 11. Molar $\text{TOC}/\text{P}_{\text{org}}$ and $\text{TOC}/\text{P}_{\text{reactive}}$ for the three sediment cores; a) euxinic core; b) chemocline core; c) oxic core. Dashed lines represent the Redfield TOC/P ratio (106:1). Grey shading marks landslide intervals.

Fig. 12. Saturation index for vivianite, siderite and pyrite in the euxinic core.

Fig. 13. Eh-pH diagram showing stability fields for different iron minerals at different depths in the euxinic core (strengite is ferric phosphate mineral: $\text{FePO}_4 \cdot 2\text{H}_2\text{O}$); a) at 0-5 cm; b) at 29.5-31.5 cm; c) enlargement of highlighted area.

Table 1. Fe extraction protocol. Steps I-III are performed sequentially on a sub-sample, and steps IV and V are performed sequentially on a separate sub-sample.

Step	Extraction details	Target Fe phases	RSD (%)
I	5 mL 0.5 M HCl (shake for 1h)	Fe(II)_{unsulf} : Extraction targets reduced solid phase Fe, including AVS and Fe(II) phosphates. Subtraction of Fe _{AVS} (step IV) gives unsulfidized solid phase Fe(II)	3
		Fe_{ox1} : Extraction also gives total Fe (i.e., Fe(II) + Fe(III)) solubilized by this technique. Subtraction of Fe(II) gives highly reducible ferric oxides such as ferrihydrite	11
II	10 mL sodium citrate/acetic acid/sodium dithionite solution (58.82 g/L sodium citrate, 20 mL/L acetic acid, 50 g/L sodium dithionite, shake for 2 h)	Fe_{ox2} : Reducible ferric oxides such as goethite and hematite	4
III	10 mL ammonium oxalate/oxalic acid (28.42g/L ammonium oxalate, 21.45 g/L oxalic acid, shake for 6h)	Fe_{mag} : Magnetite	5
IV	8 mL 50% HCl (boil for 1h)	Fe_{AVS} : Acid volatile sulfide	5
V	5 mL 1M chromous chloride dissolved in 50% HCl (boil for 1 h)	Fe_{py} : Pyrite	5

Table 2. Sequential SEDEX steps for different target P phases.

Step	Extractant	Target P phase	RSD (%)
I	5 mL 1 M MgCl ₂ (pH 8, shake for 2h) × 2	P_{sorb} : loosely sorbed P	5
	5 mL MilliQ water (shake for 2h) × 2		
II	10 mL sodium citrate/sodium bicarbonate/sodium dithionite solution (88.23 g/L sodium citrate, 84.01 g/L sodium bicarbonate, 24.38 g/L sodium dithionite, shake for 8 h)	P_{Fe} : Fe-bound P	2
	5 mL 1 M MgCl ₂ (pH 8, shake for 2 h)		
	5 mL MilliQ water (shake for 2 h)		
III	10 mL, 1 M acetate sodium (pH 4, shake for 6h)	P_{auth} : Carbonate-associated P, authigenic apatite and biogenic apatite	3
	5 mL 1 M MgCl ₂ (pH 8, shake for 2 h) × 2		
	5 mL MilliQ water (shake for 2 h)		
IV	10 mL 10% HCl (shake for 16 h)	P_{detr} : Detrital apatite and other inorganic P phases	2
V	Ash at 550 °C	P_{org} : Organic phosphorus	3
	10 mL 10% HCl (shake for 16 h)		

Figure 1

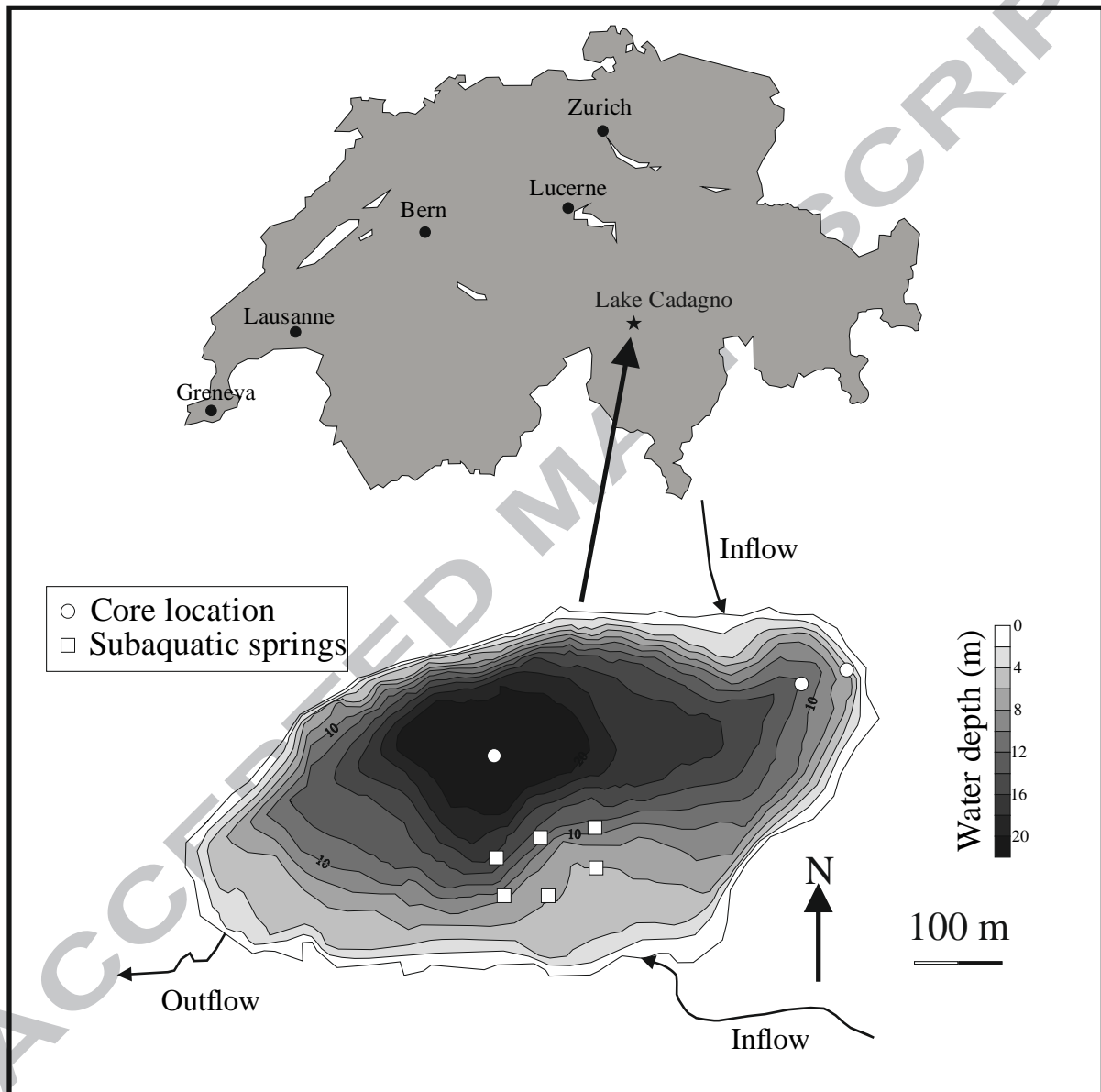


Figure 2

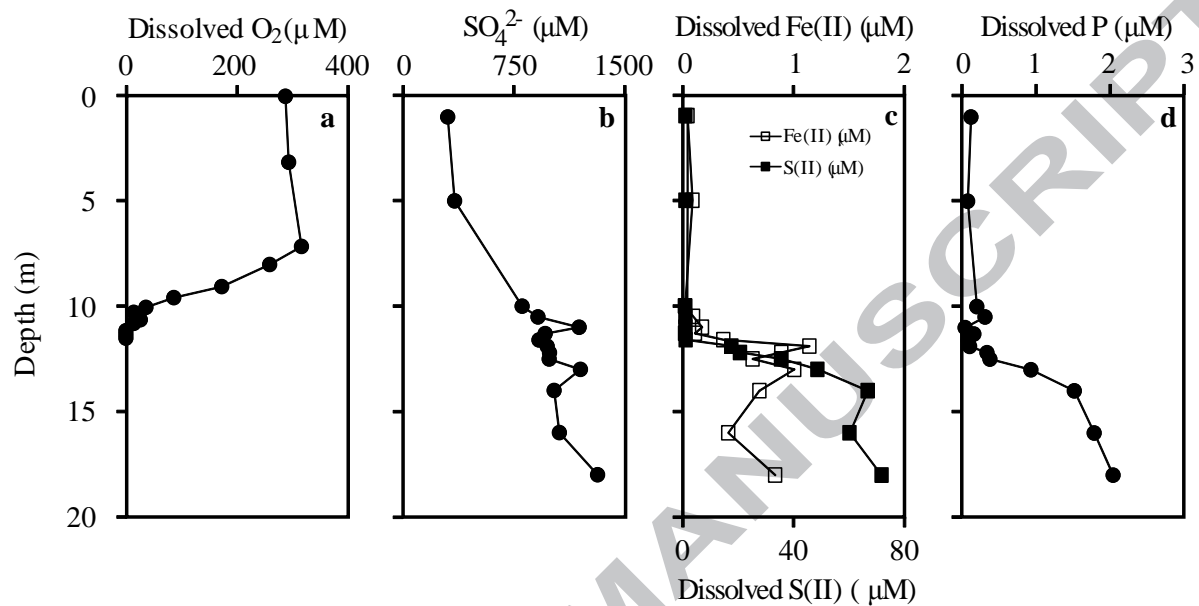


Figure 3

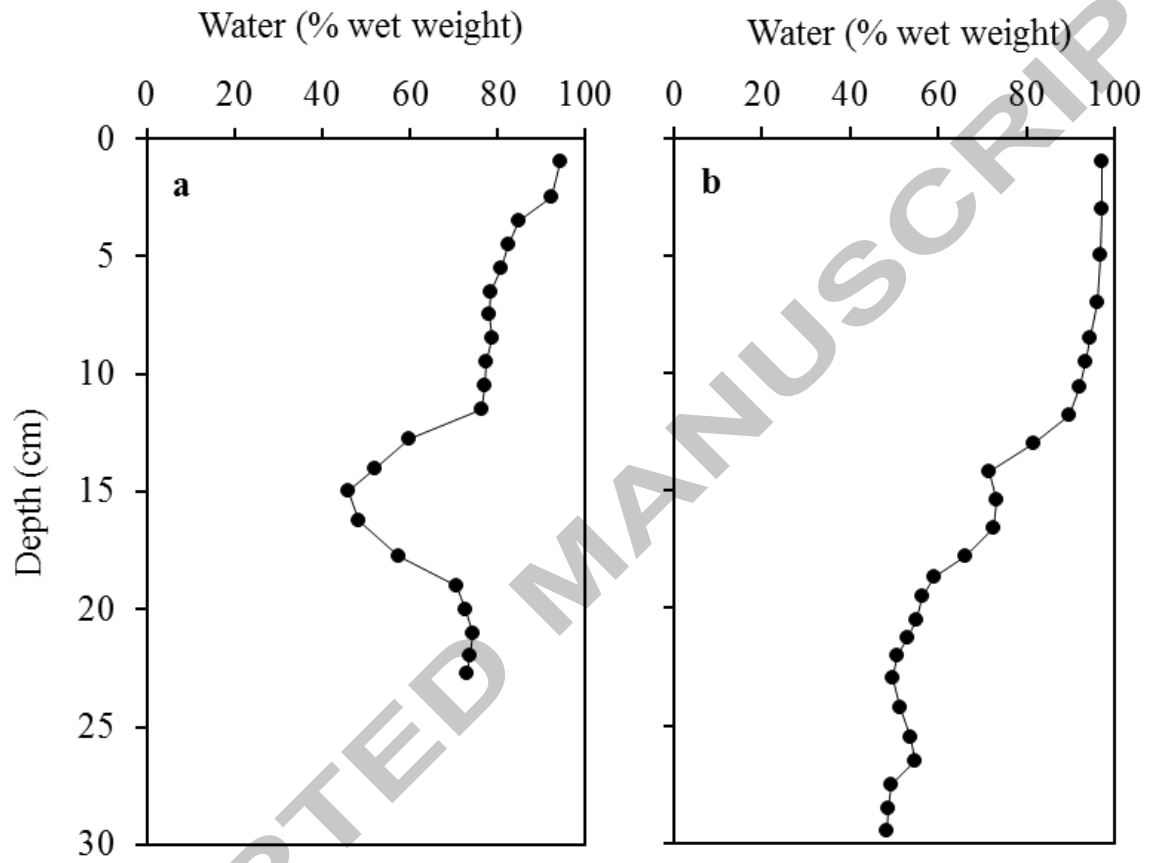


Figure 4

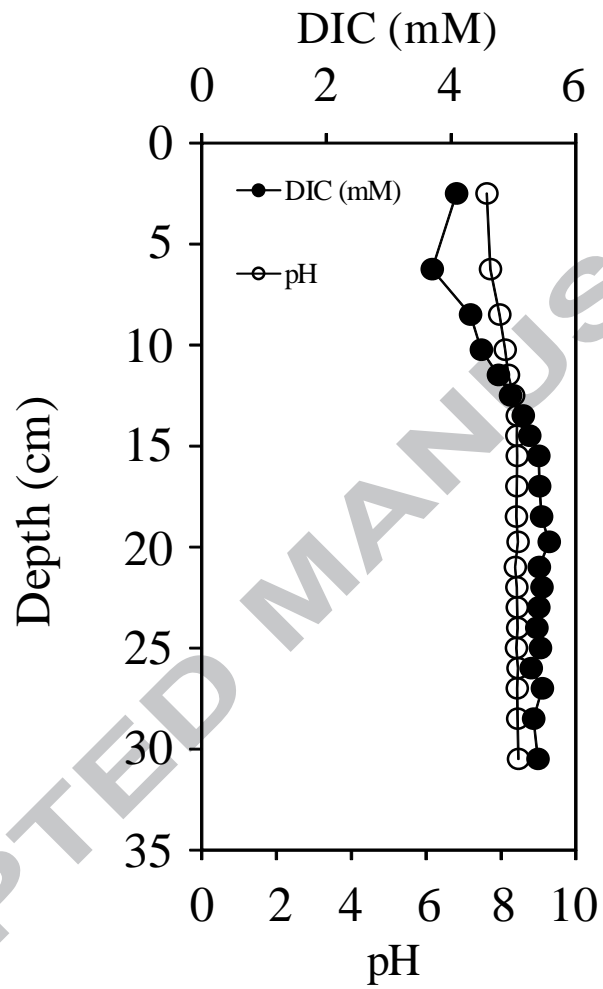


Figure 5

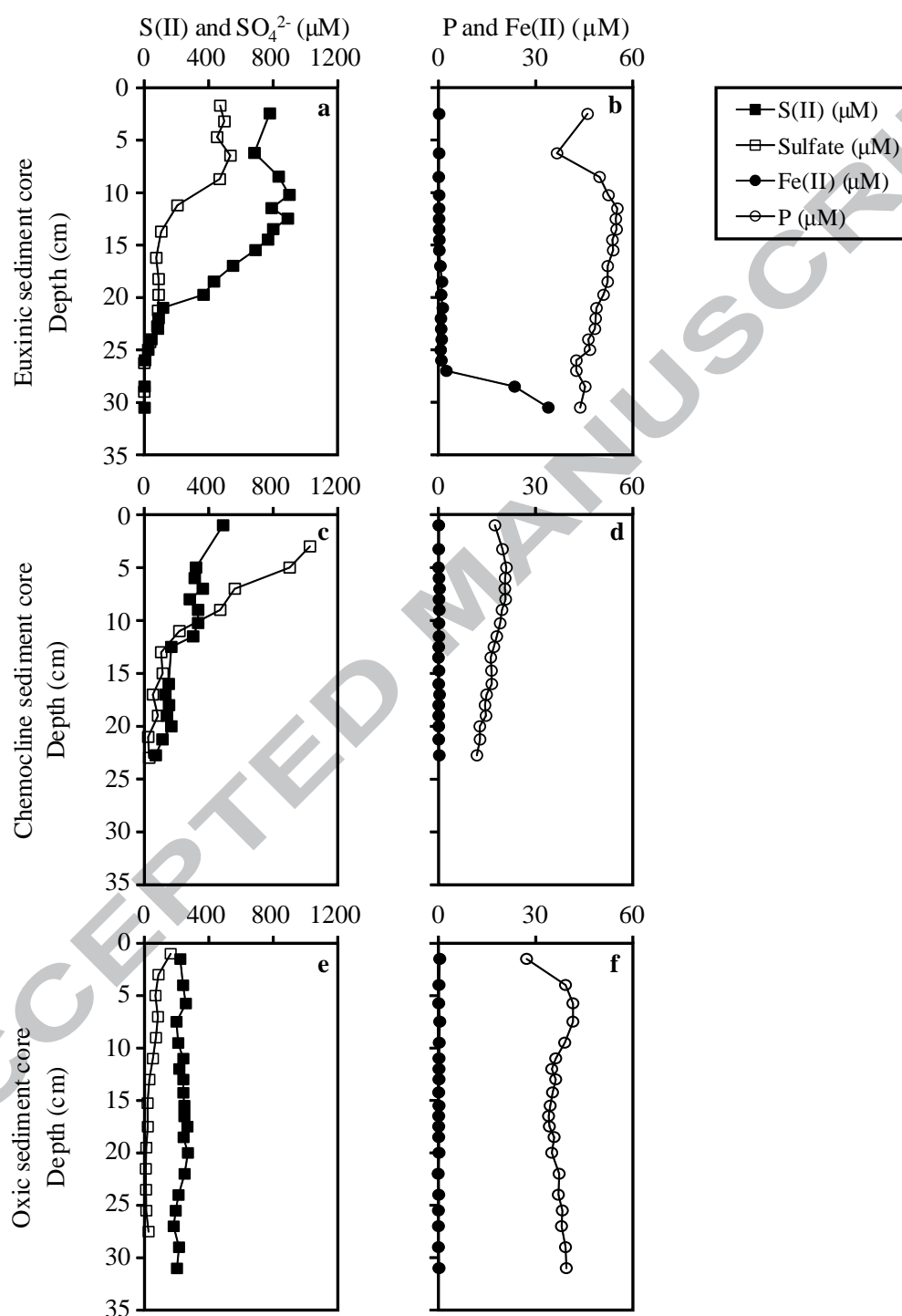


Figure 6

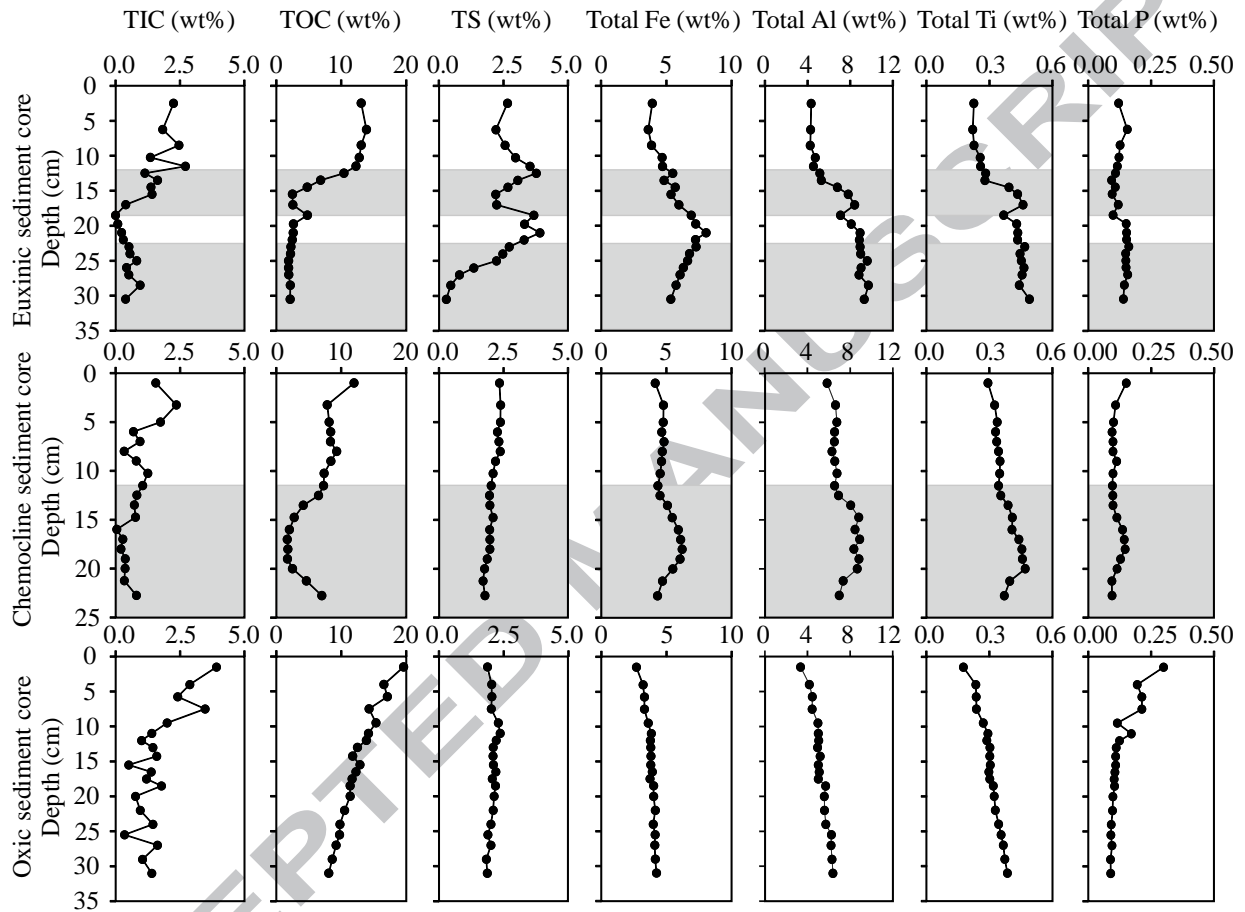


Figure 7

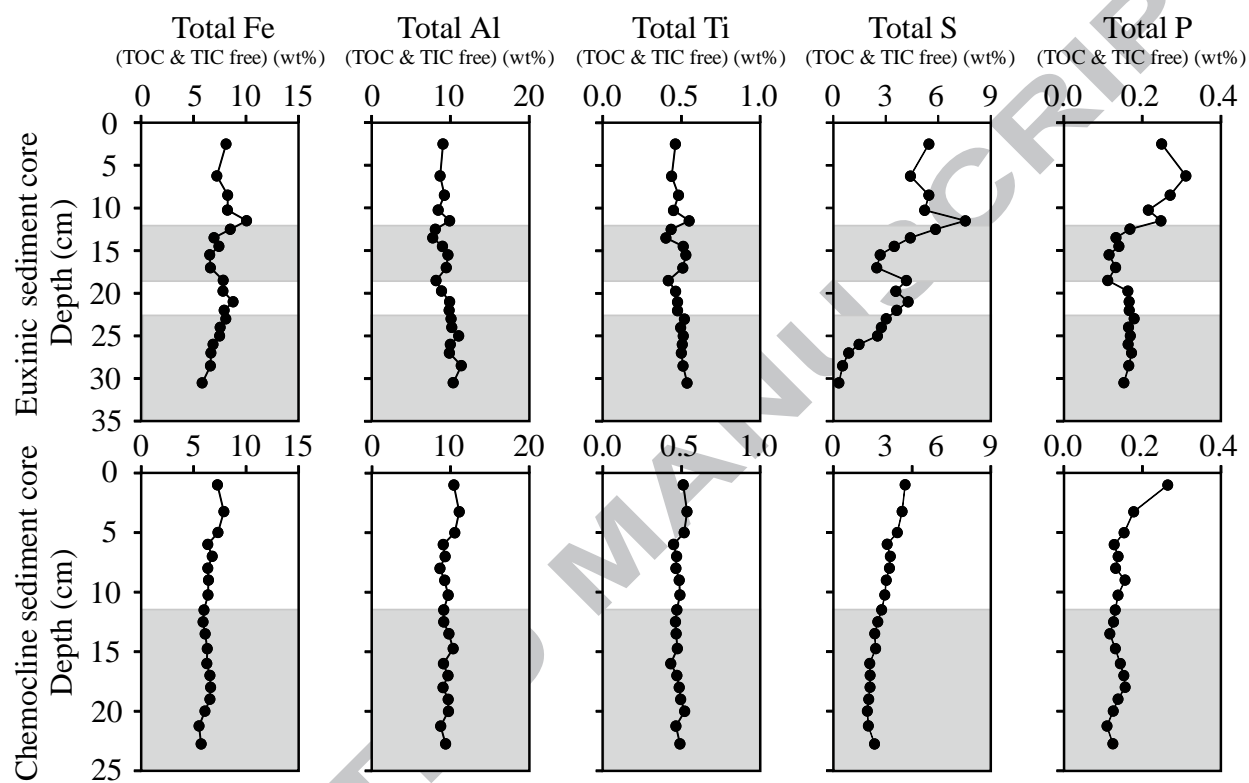


Figure 8

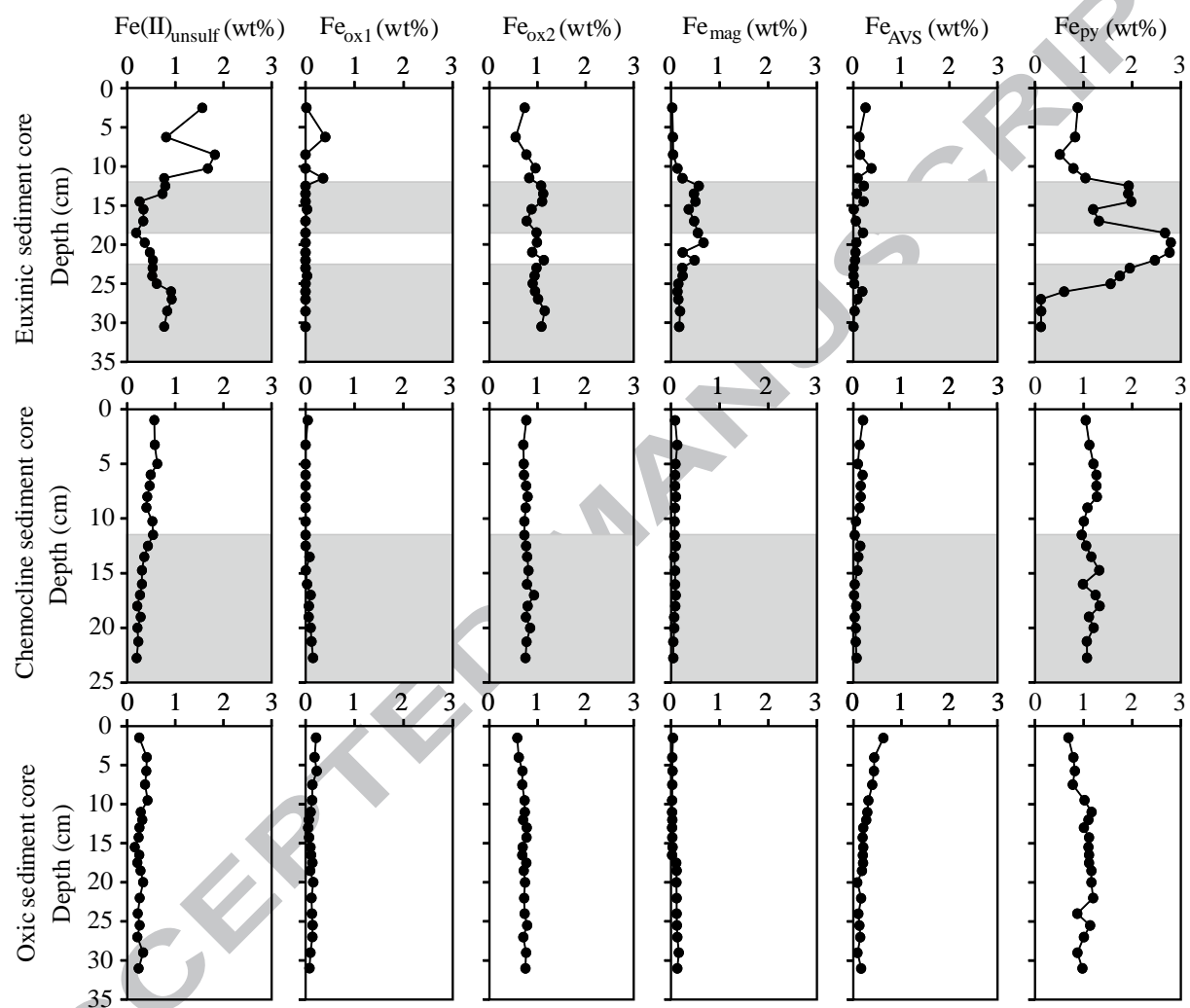


Figure 9

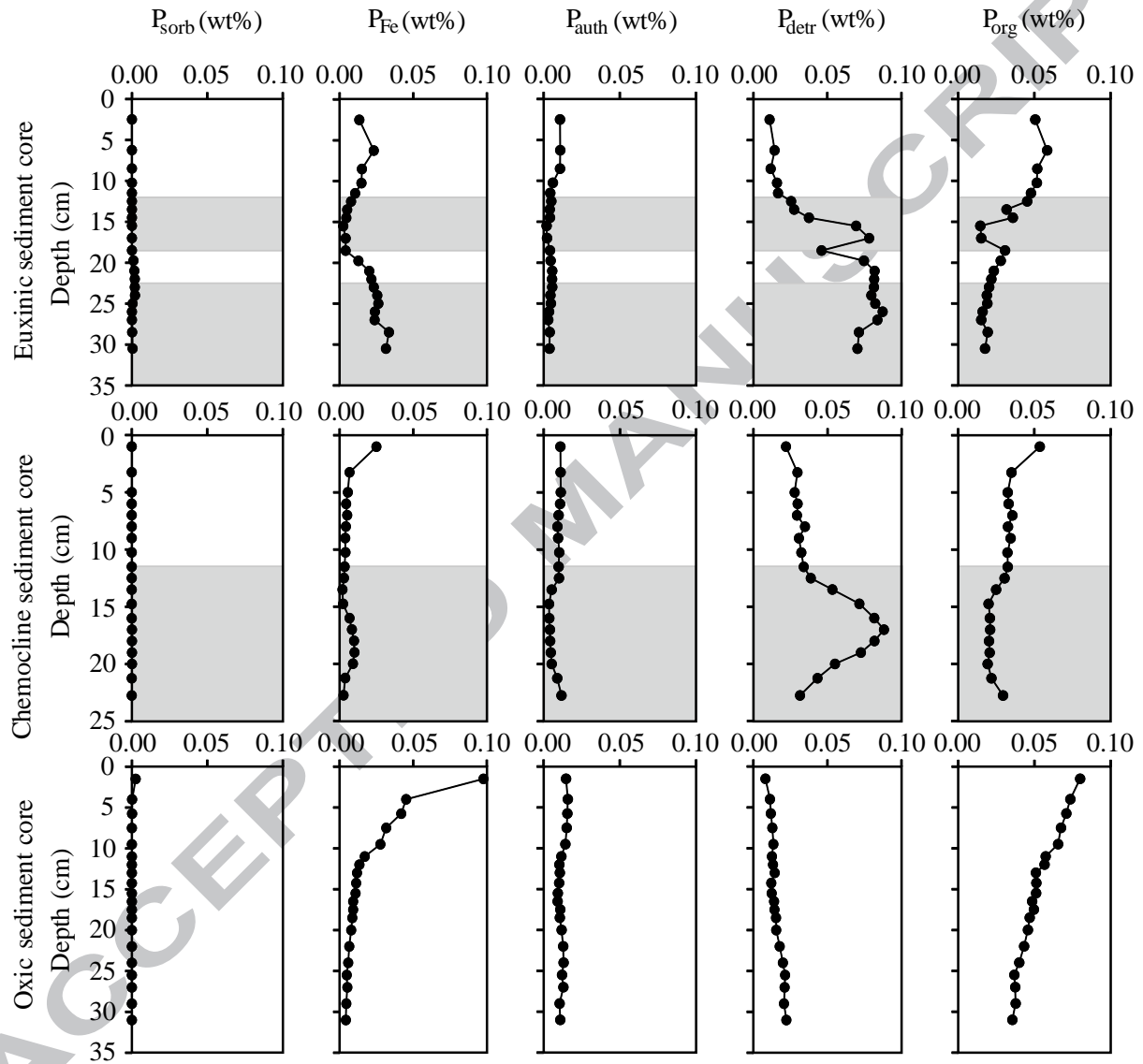


Figure 10

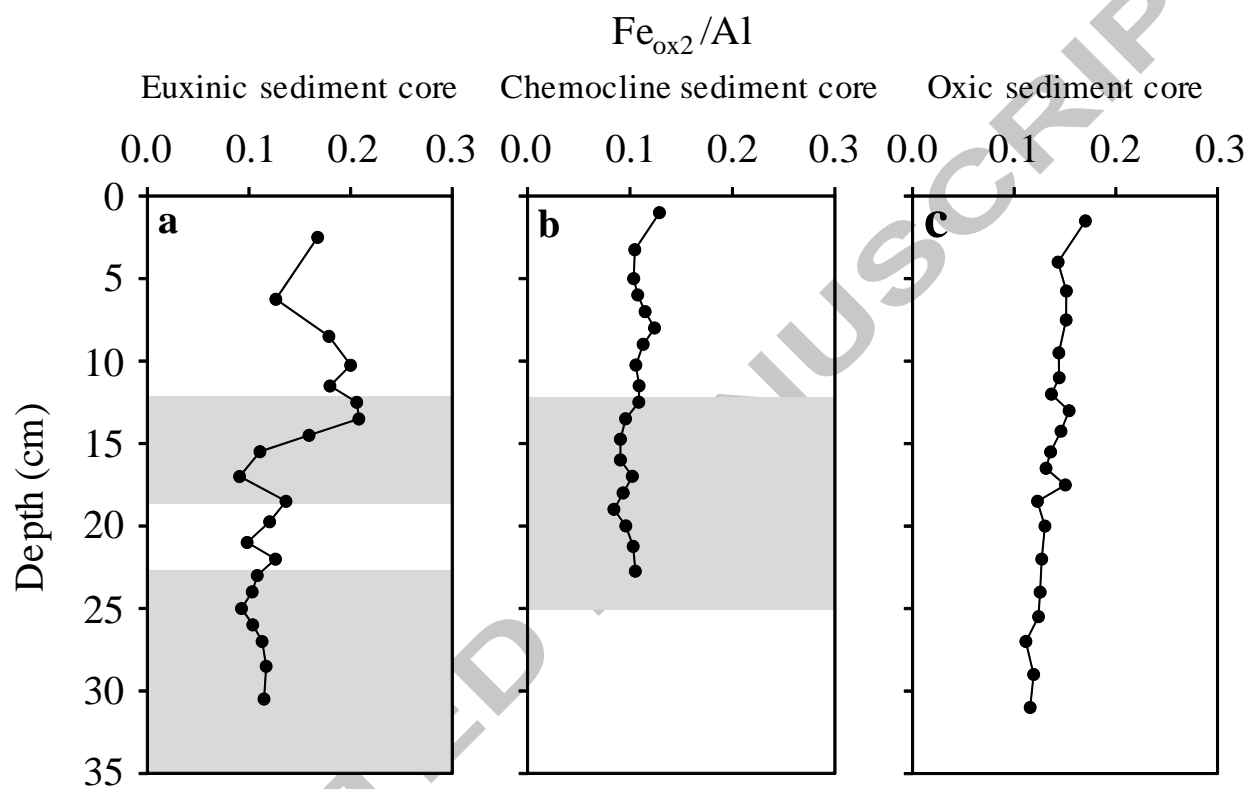


Figure 11

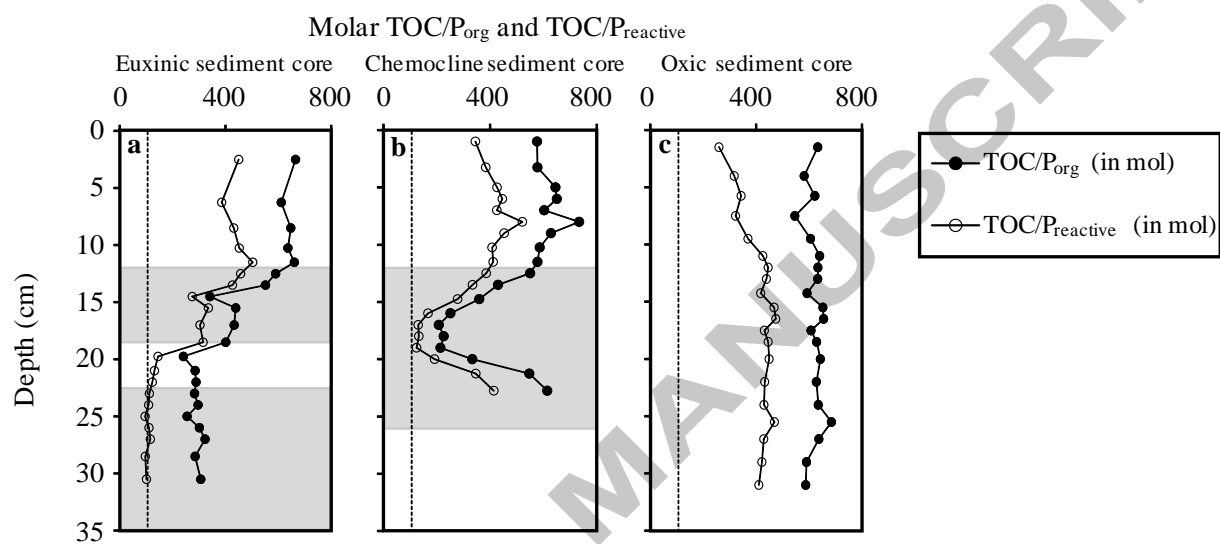


Figure 12

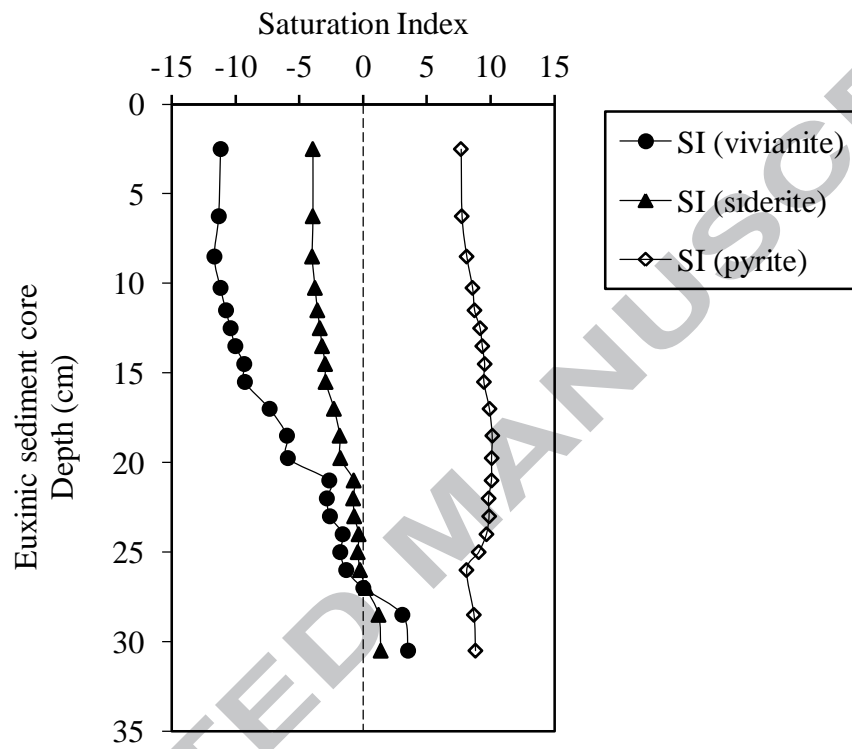


Figure 13

